Dissolved iron in the North Atlantic Ocean and Labrador Sea along the GEOVIDE section (GEOTRACES section GA01)

Manon Tonnard[1,2,3], Hélène Planquette[1], Andrew R. Bowie[2,3], Pier van der Merwe[2], Morgane Gallinari[1], Floriane Desprez de Gésincourt[1], Yoan Germain[4], Arthur Gourain[5], Marion Benetti[6,7], Gilles Reverdin[7], Paul Tréguer[1], Julia Boutorh[1], Marie Cheize[1], François Lacan[8], Jan-Lukas Menzel Barraqueta[9,10], Leonardo Pereira-Contreira[11], Rachel Shelley[1,12,13], Pascale Lherminier[14], Géraldine Sarthou[1]

1Univ Brest, CNRS, IRD, Ifremer, LEMAR, F-29280 Plouzane, France

[2]Antarctic Climate and Ecosystems – Cooperative Research Centre, University of Tasmania, Hobart, TAS 7001, Australia

[3]Institute for Marine and Antarctic Studies, University of Tasmania, Hobart, TAS 7001, Australia

[4]Laboratoire Cycles Géochimiques et ressources – Ifremer, Plouzané, 29280, France

[5]Ocean Sciences Department, School of Environmental Sciences, University of Liverpool, L69 3GP, UK

[6]Institute of Earth Sciences, University of Iceland, Reykjavik, Iceland

[7]LOCEAN, Sorbonne Universités, UPMC/CNRS/IRD/MNHN, Paris, France

[8]LEGOS, Université de Toulouse - CNRS/IRD/CNES/UPS – Observatoire Midi-Pyrénées, Toulouse, France

[9]GEOMAR Helmholtz-Zentrum für Ozeanforschung Kiel Wischhofstraße 1-3, Geb. 12 D-24148 Kiel, Germany

[10]Department of Earth Sciences, Stellenbosch University, Stellenbosch, 7600, South Africa

[11]Fundação Universidade Federal do Rio Grande (FURG), R. Luis Loréa, Rio Grande –RS, 96200-350, Brazil

[12]Dept. Earth, Ocean and Atmospheric Science, Florida State University, 117 N Woodward Ave, Tallahassee, Florida, 32301, USA

[13]School of Geography, Earth and Environmental Sciences, University of Plymouth, Drake Circus, Plymouth, PL4 8AA, UK
[14] Ifremer, Univ Brest, CNRS, IRD, Laboratoire d'Océanographie Physique et Spatiale (LOPS), IUEM, F-29280, Plouzané, France
Correspondence to: geraldine.sarthou@univ-brest.fr; helene.planquette@univ-brest.fr

Abstract.

Dissolved Fe (DFe) samples from the GEOVIDE voyage (GEOTRACES GA01, May-June 2014) in the North Atlantic Ocean were analysed using a Sea*FAST*-pico^{TM} coupled to an Element XR SF-ICP-MS and provided interesting insights on the Fe sources in this area. Overall, DFe concentrations ranged from 0.09 ± 0.01 nmol L^{-1} to 7.8 ± 0.5 nmol L^{-1}. Elevated DFe concentrations were observed above the Iberian, Greenland and Newfoundland Margins likely due to riverine inputs from the Tagus River, meteoric water inputs and sedimentary inputs. Deep winter convection occurring the previous winter provided iron-to-nitrate ratios sufficient to sustain phytoplankton growth and lead to relatively elevated DFe concentrations within subsurface waters of the Irminger Sea. Increasing DFe concentrations along the flow path of the Labrador Sea Water were attributed to sedimentary inputs from the Newfoundland Margin. Bottom waters from the Irminger Sea displayed high DFe concentrations likely due to the dissolution of Fe-rich particles in the Denmark Strait Overflow Water and the Polar Intermediate Water. Finally, the nepheloid layers located in the different basins and at the Iberian Margin were found to act as either a source or a sink of DFe depending on the nature of particles with organic particles likely releasing DFe and Mn-particles scavenging DFe.

1 Introduction

The North Atlantic Ocean is known for its pronounced spring phytoplankton blooms (Henson et al., 2009; Longhurst, 2007). Phytoplankton blooms induce the capture of aqueous carbon dioxide through photosynthesis, and conversion into particulate organic carbon (POC). This POC is then exported into deeper waters through sinking and ocean currents. Via these processes, and in conjunction with the physical carbon pump, the North Atlantic Ocean is the largest oceanic sink of anthropogenic CO_2 (Pérez et al., 2013), despite covering only 15% of global ocean area (Humphreys et al., 2016; Sabine et al., 2004) and is therefore crucial for Earth's climate.

Indeed, phytoplankton must obtain, besides light and inorganic carbon, chemical forms of essential elements, termed nutrients to be able to photosynthesise. The availability of these nutrients in the upper ocean frequently limits the activity and abundance of these organisms together with light conditions (Moore et al., 2013). In particular, winter nutrient reserves in surface waters set an upper limit for biomass accumulation during the annual spring-to-summer bloom and will influence the duration of the bloom (Follows and Dutkiewicz, 2001; Henson et al., 2009; Moore et al., 2013; 2008). Hence, nutrient depletion due to biological consumption is considered as a major factor in the decline of blooms (Harrison et al., 2013).

The extensive studies conducted in the North Atlantic Ocean through the Continuous Plankton Recorder (CPR) have highlighted the relationship between the strength of the westerlies and the displacement of the subarctic front (SAF), (which corresponds to the North Atlantic Oscillation (NAO) index (Bersch et al., 2007)), and the phytoplankton dynamics of the central North Atlantic Ocean (Barton et al., 2003). Therefore, the SAF not only delineates the subtropical gyre from the subpolar gyre but also two distinct systems in which phytoplankton limitations are controlled by different factors. In the North Atlantic Ocean, spring phytoplankton growth is largely light-limited within the subpolar gyre. Light levels are primarily set by freeze-thaw cycles of sea ice and the high-latitude extremes in the solar cycle (Longhurst, 2007). Simultaneously, intense winter mixing supplies surface waters with high concentrations of nutrients. In contrast, within the subtropical gyre, the spring phytoplankton growth is less impacted by the light regime and has been shown to be N and P-co-limited (e.g. Harrison et al., 2013; Moore et al., 2008). This is principally driven by Ekman downwelling with an associated export of nutrients out of the euphotic zone (Oschlies, 2002). Thus, depending on the location of the SAF, phytoplankton communities from the central North Atlantic Ocean will be primarily light or nutrient limited.

However, once the water column stratifies and phytoplankton are released from light limitation, seasonal high-nutrient, low chlorophyll (HNLC) conditions were reported at the transition zone between the gyres, especially in the Irminger Sea and Iceland Basin (Sanders et al., 2005). In these HNLC zones, trace metals are most likely limiting the biological carbon pump. Among all the trace metals, Fe has been recognized as the prime limiting element of North Atlantic primary productivity (e.g. Boyd et al., 2000; Martin et al., 1994; 1988; 1990). Indeed, Fe is a key element for a number of metabolic processes (e.g. Morel et al., 2008). However, the phytoplankton community has been shown to become N and/or Fe-(co)-limited in the Iceland Basin and the Irminger Sea (e.g. Nielsdóttir et al., 2009; Painter et al., 2014; Sanders et al., 2005).

In the North Atlantic Ocean, dissolved Fe (DFe) is delivered through multiple pathways such as ice-melting (e.g. Klunder et al., 2012; Tovar-Sanchez et al., 2010), atmospheric inputs (Achterberg et al., 2018; Baker et al., 2013; Shelley et al., 2015; 2017), coastal runoff (Rijkenberg et al., 2014), sediment inputs (Hatta et al., 2015), hydrothermal inputs (Achterberg et al., 2018; Conway and John, 2014) and by water mass circulation (vertical and lateral advections, e.g. Laes et al., 2003). Dissolved Fe can be regenerated through biological recycling (microbial loop, zooplankton grazing, e.g. Boyd et al., 2010; Sarthou et al., 2008). Iron is removed from the dissolved phase by biological uptake, export and scavenging throughout the water column and precipitation (itself a function of salinity, pH of seawater and ligand concentrations).

Although many studies investigated the distribution of DFe in the North Atlantic Ocean, much of this work was restricted to the upper layers (< 1000 m depth) or to one basin. Therefore, uncertainties remain on the large-scale distribution of DFe in the North Atlantic Ocean and more specifically within the subpolar gyre where few studies have been undertaken, and even fewer in the Labrador Sea. In this biogeochemically important area, high-resolution studies are still lacking for understanding the processes influencing the cycle of DFe.

The aim of this paper is to elucidate the sources and sinks of DFe, its distribution regarding water masses and assesses the links with biological activity along the GEOVIDE (GEOTRACES-GA01) transect. This transect spanned several biogeochemical provinces including the West European Basin, the Iceland Basin, the Irminger and the Labrador Seas (Fig. 1). In doing so we hope to constrain the potential long-range transport of DFe through the Deep Western Boundary Current (DWBC) via the investigation of the local processes effecting the DFe concentrations within the three

main water masses that constitute it: Iceland Scotland Overflow Water (ISOW), Denmark Strait Overflow Water (DSOW) and Labrador Sea Water (LSW).

2 Material and methods

2.1 Study area and sampling activities

Samples were collected during the GEOVIDE (GEOTRACES-GA01 section, Fig. 1) oceanographic voyage from 15 May 2014 (Lisbon, Portugal) to 30 June 2014 (St. John's, Newfoundland, Canada) aboard N/O *Pourquoi Pas?*. The study was carried out along the OVIDE line (http://www.umr-lops.fr/Projets/Projets-actifs/OVIDE, previously referred to as the WOCE A25 Greenland to Portugal section), and in the Labrador Sea (corresponding to the WOCE A01 leg 3 Greenland to Newfoundland section). The OVIDE line has been sampled every two years since 2002 in the North Atlantic (e.g. Mercier et al., 2015), and in the Labrador Sea (broadly corresponding to the WOCE A01 leg 3 Greenland to Newfoundland section). In total, 32 stations were occupied, and samples were usually collected at 22 depths, except at shallower stations close to the Iberian, Greenland and Canadian shelves (Fig. 1) where fewer samples (between 6 and 11) were collected. To avoid ship contamination of surface waters, the shallowest sampling depth was 15 m at all stations. Therefore, 'surface water samples' refers to 15m depth.

Samples were collected using a trace metal clean polyurethane powder-coated aluminium frame rosette (hereafter referred to as TMR) equipped with twenty-two 12L, externally closing, Teflon-lined, GO-FLO bottles (General Oceanics) and attached to a Kevlar® line. The cleaning protocols for sampling bottles and equipment followed the guidelines of the GEOTRACES Cookbook (www.geotraces.org, Cutter et al., 2017). After TMR recovery, GO-FLO bottles were transferred into a clean container equipped with a class 100 laminar flow hood. Samples were either taken from the filtrate of particulate samples (collected on polyethersulfone filters, 0.45 µm supor®, see Gourain et al., 2019) or after filtration using 0.2 µm filter cartridges (Sartorius SARTOBRAN® 300) due to water budget restriction (Table 1). Filtration techniques were not directly compared for the same samples, however, Wilcoxon statistical tests were performed to compare the distribution of DFe at each pair of adjacent stations where the change of filtration technique was performed (see Table 1). No significant differences were observed (p-value > 0.2) for all pairs of stations (n = 9), except between stations 11/13 and 13/15. Moreover, both filtration techniques are deemed acceptable by the GEOTRACES

guidelines. Seawater was collected in acid-cleaned 60 mL LDPE bottles, after rinsing 3 times with about 20 mL of seawater. Teflon® tubing used to connect the filter holders or cartridges to the GO-FLO bottles were washed in an acid-bath (10% v/v HCl, Suprapur®, Merck) for at least 12 h and rinsed three times with Ultra High Purity Water (UHPW > 18 MΩ.cm) prior to use. Samples were then acidified to ~ pH 1.7 with HCl (Ultrapur® Merck, 2 ‰ v/v) under a class 100 laminar flow hood inside the clean container. The sample bottles were then double bagged and stored at ambient temperature in the dark before shore-based analyses one year after collection.

Large volumes of seawater sample (referred hereafter as the in-house standard seawater) were also collected using a towed fish at around 2-3 m deep and filtered in-line inside a clean container through a 0.2 µm pore size filter capsule (Sartorius SARTOBRAN® 300) and was stored unacidified in 20-30 L LDPE carboys (Nalgene™). All the carboys were cleaned following the guidelines of the GEOTRACES Cookbook (Cutter et al., 2017). This in-house standard seawater was used for calibration on the Sea*FAST*-pico™ - SF-ICP-MS (see Section 2.2) and was acidified to ~ pH 1.7 with HCl (Ultrapur® Merck, 2 ‰ v/v) at least 24h prior to analysis.

2.2 DFe analysis with Sea*FAST*-pico™

Seawater samples were preconcentrated using a Sea*FAST*-pico™ (ESI, Elemental Scientific, USA) and the eluent was directly introduced via a PFA-ST nebulizer and a cyclonic spray chamber in an Element XR Sector Field Inductively Coupled Plasma Mass Spectrometer (Element XR SF-ICP-MS, Thermo Fisher Scientific Inc., Omaha, NE), following the protocol of Lagerström et al. (2013).

High-purity grade solutions and water (Milli-Q) were used to prepare the following reagents each day: the acetic acid-ammonium acetate buffer ($CH3COO^-$ and $NH4^+$) was made of 140 mL acetic acid (> 99% NORMATOM® - VWR chemicals) and ammonium hydroxide (25%, Merck Suprapur®) in 500 mL PTFE bottles and was adjusted to pH 6.0 ± 0.2 for the on-line pH adjustment of the samples. The eluent was made of 1.4 M nitric acid (HNO_3, Merck Ultrapur®) in Milli-Q water by a 10-fold dilution and spiked with 1 µg L^{-1} ^{115}In (SCP Science calibration standards) to allow for drift correction. Autosampler and column rinsing solutions were made of HNO_3 2.5% (v/v) (Merck Suprapur®) in Milli-Q water. The carrier solution driven by the syringe pumps to move the sample and buffer through the flow injection system was made in the same way.

All reagents, standards, samples, and blanks were prepared in acid cleaned low density polyethylene (LDPE) or Teflon fluorinated ethylene propylene (FEP) bottles. Bottles were cleaned following the GEOTRACES protocol (Cutter et al., 2017).

Mixed element standard solution was prepared gravimetrically using high purity standards (Fe, Mn, Cd, Co, Zn, Cu, Pb; SCP Science calibration standards) in HNO_3 3% (v/v) (Merck Ultrapur®). The distribution of the trace metals other than Fe will be reported elsewhere (Planquette et al., in prep.). A six-point calibration curve was prepared by standard additions of the mixed element standard to our acidified in-house standard and ran at the beginning, the middle and the end of each analytical session. Each analytical session consisted of about fifty samples. Final concentrations of samples and procedural blanks were calculated from In-normalized data. Data were blank-corrected by subtracting an average acidified Milli-Q blank that were pre-concentrated on the Sea*FAST*-pico™ in the same way as the samples and seawater standards. The errors associated to each sample were calculated as the standard deviation for five measurements of low-Fe seawater samples. The mean Milli-Q blank was equal to 0.08 ± 0.09 nmol L^{-1} (n = 17) considering all analytical sessions. The detection limit, calculated for a given run as three times the standard deviation of the Milli-Q blanks, was on average 0.05 ± 0.05 nmol L^{-1} (n = 17). Reproducibility was assessed through the standard deviation of replicate samples (every 10th sample was a replicate) and the average of the in-house standard seawater, and was equal to 17% (n = 84). Accuracy was determined from the analysis of consensus (SAFe S, GSP) and certified (NASS-7) seawater matrices (see Table 2) and in-house standard seawater (DFe = 0.42 ± 0.07 nmol L^{-1}, n = 84). Note that all the DFe values were generated in nmol kg^{-1} using the Sea*FAST*-pico™ coupled to an Element XR SF-ICP-MS and were converted to nmol L^{-1} using the actual density (in kg L^{-1}) of each seawater sample (Table 1) to be directly comparable with literature.

2.3 Meteoric water and sea ice fraction calculation

We considered the different contributions of, Sea-Ice Melt (SIM), Meteoric Water (MW), and saline seawater, at Stations 53, 61 and 78 using the procedure and mass balance calculations that are fully described in Benetti et al. (2016). Briefly,we considered two types of seawater, namely Atlantic Water (AW) and Pacific Water (PW). The relative proportions of AW () and PW () are calculated based on the distinctive nitrogen to phosphorus (N-P) relationships for the two water masses (Jones et al., 1998) as follows (e.g. Sutherland et al., 2009):

$$f_{PW} = \frac{N^m - N^{AW}}{N^{PW} - N^{AW}} \quad \text{(eq.1)}$$

where is the measured dissolved inorganic nitrogen, and are the values for pure Atlantic and Pacific water estimated from Jones et al. (1998), respectively. and values are calculated by substituting the PO_4^m value in the equation of the pure AW and PW N-P lines from Jones et al. (1998). However, during GEOVIDE, the phosphate depleted near-surface values led to unrealistic lower than just below the subsurface. Therefore, for all surface samples, the estimates were replaced by the values at 100 m.. Then, the surface values were adjusted by a factor of dilution proportional to the sample salinity.

After estimating the relative proportions of AW () and PW () and their respective salinity and $\delta^{18}O$ affecting each samples, the contribution of SIM and MW can be determined using measured salinity () and $\delta^{18}O$ (). The mass balance calculations are presented below:

$$f_{AW} + f_{PW} + f_{MW} + f_{SIM} = 1 \text{ (eq.2)}$$

$$f_{AW}.S_{AW} + f_{PW}.S_{PW} + f_{MW}.S_{MW} + f_{SIM}.S_{SIM} = S_m \text{ (eq.3)}$$

$$f_{AW}.\delta O^{18}_{AW} + f_{PW}.\delta O^{18}_{PW} + f_{MW}.\delta O^{18}_{MW} + f_{SIM}.\delta O^{18}_{SIM} = \delta O^{18}_{m} \text{ (eq.4)}$$

where f_{AW}, f_{PW}, f_{MW}, f_{SIM} are the relative fraction of AW, PW, MW, and SIM. To calculate the relative fractions of AW, PW, MW and SIM we used the following end-members: = 35, = +0.18‰ (Benetti et al., 2016); = 32.5, = -1‰ (Cooper et al., 1997; Woodgate and Aagaard, 2005); = 0, = -18.4‰ (Cooper et al., 2008); = 4, = +0.5‰ (Melling and Moore, 1995).

Negative sea-ice fractions indicated a net brine release while positive sea-ice fractions indicated a net sea-ice melting. Note that for stations over the Greenland Shelf, we assumed that Pacific Water (PW) contribution was negligible for the calculations, supported by the very low PW fractions found at Cape Farewell in May 2014 (see Figure B1 in Benetti et al., 2017), while for station 78, located on the Newfoundland shelf, we used nutrient measurements to calculate the PW fractions, following the approach from Jones et al. (1998) (the data are published in Benetti et al., 2017).

2.4 Ancillary measurements and mixed layer depth determination

Potential temperature (θ), salinity (S), dissolved oxygen (O_2) and beam attenuation data were retrieved from the CTD sensors (CTD SBE911 equipped with a SBE-43) that were deployed on a stainless steel rosette.Salinity profiles were calibrated using 1228 samples taken from the GO-FLO bottles, leading to a precision of 0.002 psu. The O_2 data could not be directly calibrated with GO-FLO samples, due to a the sampling time being too long, so the calibrated O2 profiles acquired by the classic CTD at the same station were used to calibrate the O2 profiles of the TMR CTD, with a precision estimated at 3 µmol/kg. Nutrient and total Chlorophyll-*a* (TChl-*a*) samples were collected using the classic CTD at the same stations as for the TMR. We used the data from the stainless steel

rosette casts that were deployed immediately before or after our TMR casts. Pigments were separated and quantified following an adaptation of the method described by van Heukelem and Thomas (2001) and the analytical procedure used is described in Ras et al. (2008). The method adaptation allowed for higher sensitivity in the analysis of low phytoplankton biomass waters (see Ras et al., 2008). Briefly, frozen filters were extracted at -20°C in 3 mL of methanol (100%), sonicated and then clarified by vacuum filtration through Whatman GF/F filters. The total extraction time was 2 hours. The extracts were then analysed by HPLC with a complete Agilent Technologies system 1200 (comprising LC Chemstation software, a degasser, a binary pump, a refrigerated autosampler, a column thermostat and a diode array detector) when possible on the same day as extraction. The sample extracts were premixed (1:1) with a tetrabutylammonium acetate (TBAA) buffer solution (28 nM) prior to injection in the HPLC. The mobile phase was a mix between a solution (A) of TBAA 28 mM:methanol (30:70, v:v) and a solution (B) of 100% methanol (i.e. the organic solvent) with varying proportions during analysis. After elution, pigment concentrations (in mg m-3) were calculated according to Beer-Lambert's law (i.e. A = εLC) from the peak areas with an internal standard correction (Vitamin E acetate, Sigma) and an external standard calibration (DHI Water and Environment, Denmark). This method allowed the detection of 23 phytoplankton pigments. The detection limits, defined as three times the signal:noise ratio for a filtered volume of 1 L, was 0.0001 mg.m-3 for total chlorophyll-a (TChl-a) and its injection precision was 0.91%

All these data are available on the LEFE/CYBER database (http://www.obs-vlfr.fr/proof/php/geovide/geovide.php).

The mixed layer depth (Z_m) for each station was calculated using the function "calculate.mld" (part of the "rcalcofi" package, Ed Weber at NOAA SWFSC) created by Sam McClathie (NOAA Federal, 30th December 2013) for R software and where Z_m is defined as an absolute change in the density of seawater at a given temperature ($\Delta\sigma_\theta \geq 0.125$ kg m^{-3}) with respect to an approximately uniform region of density just below the ocean surface (Kara et al., 2000). In addition to the density criterion, the temperature and salinity profiles were inspected at each station for uniformity within this layer. When they were not uniform, the depth of any perturbation in the profile was chosen as the base of the Z_m (Table 1).

2.5 Statistical analysis

All statistical approaches, namely the comparison between the pore size used for filtration, correlations and Principal Component Analysis (PCA), were performed using the R statistical software (R development Core Team 2012). For all the results, p-values were calculated against the threshold value alpha (α), that we assigned at 0.05, corresponding to a 95% level of confidence. For all data sets, non-normal distributions were observed according to the Shapiro-Wilk test. Therefore, the significance level was determined with a Wilcoxon test.

All sections and surface layer plots were prepared using Ocean Data View (Schlitzer, 2016).

2.6 Water mass determination and associated DFe concentrations

The water mass structure in the North Atlantic Ocean from the GEOVIDE voyage was quantitatively assessed by means of an extended Optimum Multi-Parameter (eOMP) analysis with 14 water masses (for details see García-Ibáñez et al., 2015; this issue). Using this water mass determination, DFe concentrations were considered as representative of a specific water mass only when the contribution of this specific water mass was higher than 60% of the total water mass pool.

2.7 Database

The complete database of dissolved Fe is available in the electronic supplement www.biogeosciences.net. Overall, 540 data points of dissolved Fe are reported, among which 511 values are used in this manuscript. The remaining 29 values (5.7% of the total dataset) are flagged as (suspect) outliers. These 29 outliers, flagged as “3” in the table, were not used in figures and in the interpretation of this manuscript . The criteria for rejection were based on the comparison with other parameters measured from the same GO-FLO sampler, and curve fitting versus samples collected above and below the suspect sample. The complete data set will be available in national and international databases (LEFE-CYBER, http://www.obs-vlfr.fr/proof/index2.php, and GEOTRACES http://www.bodc.ac.uk/geotraces/).

3 Results

293 **3.1 Hydrography**

294 The hydrology and circulation of the main water masses along the OVIDE section in the North Atlantic
295 Subpolar Gyre and their contribution to the Atlantic Meridional Overturning Circulation (AMOC) have
296 been described using an eOMP analysis by García-Ibáñez et al., (2015; 2018) and Zunino et al.
297 (2017). For a schematic of water masses, currents and pathways, see Daniault et al. (2016). Hereafter
298 we summarise the main features (Fig. 1 and 2).
299
300 *Upper waters (~ 0 – 800 m)* - The cyclonic circulation of Eastern North Atlantic Central Water
301 (ENACW) ($12.3 < \theta < 16°C$, $35.66 < S < 36.2$, $241 < O_2 < 251$ µmol kg^{-1}) occupied the water column
302 from 0 to ~ 800 m depth from stations 1 to 25 representing 60% of the water mass pool. The sharp
303 Subarctic Front (between stations 26 and 29), caused by the northern branch of the North Atlantic
304 Current (NAC) separated the cyclonic subpolar from the anticyclonic subtropical gyre domains at 50°N
305 and 22.5°W. ENACW were also encountered to a lesser extent and only in surface waters (from 0 to ~
306 100 m depth) between stations 29 and 34 (representing less than 40% of the water mass pool). West
307 of the Subarctic Front, Iceland SubPolar Mode Water (IcSPMW, $7.07 < \theta < 8°C$, $35.16 < S < 35.23$,
308 $280 < O_2 < 289$ µmol kg^{-1}) was encountered from stations 34-40 (accounting for more than 45% of the
309 water mass pool from 0 to ~ 800 m depth) and Irminger SubPolar Mode Water (IrSPMW, $\theta \approx 5°C$, $S \approx$
310 35.014) from stations 42-44 (representing to 40% of the water mass pool from 0 to ~ 250 m depth)
311 and stations 49 and 60 (accounting for 40% of the water mass pool down to 1300 m depth). IcSPMW
312 was also observed within the Subtropical gyre (stations 11-26), subducted below ENACW up to1000
313 m depth. Stations 63 (> ~ 200 m depth) and 64 (from surface down to ~ 500 m depth) exhibited a
314 contribution of the IrSPMW higher than 45%. Stations 44, 49 and 60, from the Irminger Sea, and 63
315 from the Labrador Sea were characterised by lower sea-surface salinity ranges (S = [34.636, 34.903],
316 stations 63 and 60, respectively), likely due to ice melting and meteoric water inputs. Subarctic
317 Intermediate Water (SAIW, $4.5 < \theta < 6.0°C$, $34.70 < S < 34.80$) contributed to more than 40% of the
318 water mass pool in the Iceland Basin between the surface and ~ 400 m depth at stations 29 and 32
319 and throughout the water column of stations 53, 56 and 61 and from surface down to ~ 200 m depth at
320 station 63. From stations 68 to 78 surface waters were characterized by a minimum of salinity and a
321 maximum of oxygen ($S = 34.91$, $O_2 = 285$ µmol kg^{-1}, $\theta \approx 3°C$) and corresponded to the newly formed
322 Labrador Sea Water (LSW). The LSW was also observed in surface waters of station 44 with a similar
323 contribution than IrSPMW (~ 40%).

Intermediate waters (~ 800 – 1400 m) - Mediterranean Outflow Water (MOW), distinguishable from surrounding Atlantic Water by its high salinity tongue (up to 36.2), a minimum of oxygen (O_2 = 210 µmol kg^{-1}) and relatively high temperatures (up to 11.7°C) was observed from station 1 to 21 between 800 and 1400 m depth at a neutral density ranging from 27.544 to 27.751 kg m^{-3} with the maximum contribution to the whole water mass pool seen at station 1 (64 ± 6%). Its main core was located at ~ 1200 m depth off the Iberian shelf from stations 1 to 11 and then gradually rising westward due to mixing with LSW within the North Atlantic subtropical gyre and a contribution of this water mass decreasing until station 21 down to 10-20%. LSW (27.763 < neutral density < 27.724 kg m^{-3}) was sourced from SPMW after intense heat loss and led to its deep convection. During GEOVIDE, LSW formed by deep convection the previous winter was found at several stations in the Labrador Sea (68, 69, 71 and 77). After convecting, LSW splits into three main branches with two main cores separated by the Reykjanes Ridge (stations 1-32, West European and Iceland Basins; stations 40-60, Irminger Sea), and the last one entering the West European Basin (Zunino et al., 2017).

Overflows and Deep waters (~ 1400 - 5500 m) - North East Atlantic Deep Water (NEADW, 1.98 < θ < 2.50°C, 34.895 < S < 34.940) was the dominant water mass in the West European Basin at stations 1-29 from 2000 m depth to the bottom and is characterized by high silicic acid (42 ± 4 µmol L^{-1}), nitrate (21.9 ± 1.5 µmol L^{-1}) concentrations and lower oxygen concentration (O_2 ≈ 252 µmol kg^{-1}) (see Sarthou et al., 2018). The core of the NEADW (stations 1-13) was located near the seafloor and gradually decreased westward. Polar Intermediate Water (PIW, θ ≈ 0°C, S ≈ 34.65) is a ventilated, dense, low-salinity water intrusion to the deep overflows within the Irminger and Labrador Seas that is formed at the Greenland shelf. PIW represents only a small contribution to the whole water mass pool (up to 27%) and was observed over the Greenland slope at stations 53 and 61 as well as in surface waters from station 63 (from 0 to ~ 200 m depth), in intermediate waters of stations 49, 60 and 63 (from ~ 500 to ~ 1500 m depth) and in bottom waters of stations 44, 68, 69, 71 and 77 with a contribution higher than 10%. Iceland Scotland Overflow Water (ISOW, θ ≈ 2.6°C, S ≈ 34.98) is partly formed within the Arctic Ocean by convection of the modified Atlantic water. ISOW comes from the Iceland-Scotland sills and flows southward towards the Charlie-Gibbs Fracture Zone (CGFZ) and Bight Fracture Zone (BFZ) (stations 34 and 36) after which it reverses its flowing path northward and enters the Irminger Sea (stations 40 and 42) to finally reach the Labrador Sea close to the Greenland

coast (station 49, station 44 being located in between this two opposite flow paths). Along the eastern (stations 26-36) and western (stations 40-44) flanks of the Reykjanes Ridge, ISOW had a contribution higher than 50% to the water mass pool. ISOW was observed from 1500 m depth to the bottom of the entire Iceland Basin (stations 29-38) and from 1800 to 3000 m depth within the Irminger Sea (stations 40-60). ISOW, despite having a fraction lower than 45% above the Reykjanes Ridge (station 38), was the main contributor to the water mass pool from 1300 m depth down to the bottom. ISOW was also observed within the Labrador Sea from stations 68 to 77. Finally, the deepest part of the Irminger (stations 42 and 44) and Labrador (stations 68-71) Seas were occupied by Denmark Strait Overflow Water (DSOW, $\theta \approx 1.30°C$, $S \approx 34.905$).

3.2 Ancillary data

3.2.1 Nitrate

Surface nitrate (NO_3^-) concentrations (García-Ibáñez et al., 2018; Pérez et al., 2018; Sarthou et al., 2018) ranged from 0.01 to 10.1 µmol L^{-1} (stations 53 and 63, respectively). There was considerable spatial variability in NO_3^- surface distributions with high concentrations found in the Iceland Basin and Irminger Sea (higher than 6 µmol L^{-1}), as well as at stations 63 (10.1 µmol L^{-1}) and 64 (5.1 µmol L^{-1}), and low concentrations observed in the West European Basin, in the Labrador Sea and above continental margins. The low surface concentrations in the West European Basin ranged from 0.02 (station 11) to 3.9 (station 25) µmol L^{-1}. Station 26 delineating the extreme western boundary of the West European Basin exhibited enhanced NO_3^- concentrations as a result of mixing between ENACW and IcSPMW, although these surface waters were dominated by ENACW. In the Labrador Sea (stations 68-78) low surface concentrations were observed with values ranging from 0.04 (station 68) to 1.8 (station 71) µmol L^{-1}. At depth, the lowest concentrations (lower than 15.9 µmol L^{-1}) were measured in ENACW (~ 0 - 800 m depth) and DSOW (> 1400 m depth), while the highest concentrations were measured within NEADW (up to 23.5 µmol L^{-1}), and in the mesopelagic zone of the West European and Iceland Basins (higher than 18.4 µmol L^{-1}).

3.2.2 Chlorophyll-*a*

Overall, most of the phytoplankton biomass was localised above 100 m depth with lower total chlorophyll-*a* (TChl-*a*) concentrations South of the Subarctic Front and higher at higher latitudes (see supplementary material Fig. S1). While comparing TChl-*a* maxima considering all stations, the lowest value (0.35 mg m^{-3}) was measured within the West European Basin (station 19, 50 m depth) while the highest values were measured at the Greenland (up to 4.9 mg m^{-3}, 30 m depth, station 53 and up to 6.6 mg m^{-3}, 23 m depth, station 61) and Newfoundland (up to 9.6 mg m^{-3}, 30 m depth, station 78) margins.

3.3 Dissolved Fe concentrations

Dissolved Fe concentrations (see supplementary material Table S1) ranged from 0.09 ± 0.01 nmol L^{-1} (station 19, 20 m depth) to 7.8 ± 0.5 nmol L^{-1} (station 78, 371 m depth) (see Fig. 3). Generally, vertical profiles of DFe for stations above the margins (2, 4, 53, 56, 61, and 78) showed an increase with depth, although sea-surface maxima were observed at stations 2, 4 and 56. For these margin stations, values ranged from 0.7 to 1.0 nmol L^{-1} in the surface waters. Concentrations increased towards the bottom, with more than 7.8 nmol L^{-1} measured at station 78, approximately 1-3 nmol L^{-1} for stations 2, 4, 53, and 61, and just above 0.4 nmol L^{-1} for station 56 (Fig. 4). Considering the four oceanic basins, mean vertical profiles (supplementary material Fig. S2) showed increasing DFe concentrations down to 3000 m depth followed by decreasing DFe concentrations down to the bottom. Among deep-water masses, the lowest DFe concentrations were measured in the West European Basin. The Irminger Sea displayed the highest DFe concentrations from 1000 m depth to the bottom relative to other basins at similar depths (Fig. 3 and supplementary material Fig. S2). In the Labrador Sea, DFe concentrations were low and relatively constant at about 0.87 ± 0.06 nmol L^{-1} from 250 m to 3000 m depth (Fig. S2). Overall, surface DFe concentrations were higher (0.36 ± 0.18 nmol L^{-1}) in the North Atlantic Subpolar gyre (above 52°N) than in the North Atlantic Subtropical gyre (0.17 ± 0.05 nmol L^{-1}). The surface DFe concentrations were generally smaller than 0.3 nmol L^{-1}, except for few stations in the Iceland Basin (stations 32 and 38), Irminger (stations 40 and 42) and Labrador (station 63) Seas, where values ranged between 0.4-0.5 nmol L^{-1}.

3.4 DFe signatures in water masses

In the Labrador Sea, IrSPMW exhibited an average DFe concentration of 0.61 ± 0.21 nmol L^{-1} (n=14). DFe concentrations in the LSW were the lowest in this basin, with an average value of 0.71 ± 0.27 nmol L^{-1} (n=53) (see supplementary material Fig. S3). Deeper, ISOW displayed slightly higher average DFe concentrations (0.82 ± 0.05 nmol L^{-1}, n=2). Finally, DSOW had the lowest average (0.68 ± 0.06 nmol L^{-1}, n=3, see supplementary material Fig. S3) and median (0.65 nmol L^{-1}) DFe values for intermediate and deep waters.

In the Irminger Sea, surface waters were composed of SAIW (0.56 ± 0.24 nmol L^{-1}, n=4) and IrSPMW (0.72 ± 0.32 nmol L^{-1}, n=34). The highest open-ocean DFe concentrations (up to 2.5 ± 0.3 nmol L^{-1}, station 44, 2600 m depth) were measured within this basin. In the upper intermediate waters, LSW was identified only at stations 40 to 44, and had the highest DFe values with an average of 1.2 ± 0.3 nmol L^{-1} (n=14). ISOW showed higher DFe concentrations than in the Iceland Basin (1.3 ± 0.2 nmol L^{-1}, n=4). At the bottom, DSOW was mainly located at stations 42 and 44 and presented the highest average DFe values (1.4 ± 0.4 nmol L^{-1}, n=5) as well as the highest variability from all the water masses presented in this section (see supplementary material Fig. S3).

In the Iceland Basin, SAIW and IcSPMW displayed similar averaged DFe concentrations (0.67 ± 0.30 nmol L^{-1}, n=7 and 0.55 ± 0.34 nmol L^{-1}, n=22, respectively). Averaged DFe concentrations were similar in both LSW and ISOW, and higher than in SAIW and IcSPMW (0.96 ± 0.22 nmol L^{-1}, n=21 and 1.0 ± 0.3 nmol L^{-1}, n=10, respectively, see supplementary material Fig. S3).

Finally, in the West European Basin, DFe concentrations in ENACW were the lowest of the whole section with an average value of 0.30 ± 0.16 nmol L^{-1} (n=64). MOW was present deeper in the water column but was not characterized by particularly high or low DFe concentrations relative to the surrounding Atlantic waters (see supplementary material Fig. S3). The median DFe value in MOW was very similar to the median value when considering all water masses (0.75 and 0.77 nmol L^{-1}, respectively, Fig. S3). LSW and IcSPMW displayed slightly elevated DFe concentrations compared to the overall median with mean values of 0.82 ± 0.08 (n=28) and 0.80 ± 0.04 (n=8) nmol L^{-1}, respectively. The DFe concentrations in NEADW were relatively similar to the DFe median value of the GEOVIDE voyage (0.71 and 0.77 nmol L^{-1}, respectively, Fig. S3.

4 Discussion

In the following sections, we will first discuss the high DFe concentrations observed throughout the water column of stations 1 and 17 located in the West European Basin (Section 4.1), then, the relationship between water masses and the DFe concentrations (Section 4.2) in intermediate (Section 4.2.2 and 4.2.3) and deep (Section 4.2.4 and 4.2.5) waters. We will also discuss the role of wind (Section 4.2.1), rivers (Section 4.3.1), meteoric water and sea-ice processes (Section 4.3.2), atmospheric deposition (Section 4.3.3) and sediments (Section 4.4) in delivering DFe. Finally, we will discuss the potential Fe limitation using DFe:NO_3^- ratios (Section 4.5).

4.1 High DFe concentrations at station 1 and 17

Considering the entire section, two stations (stations 1 and 17) showed irregularly high DFe concentrations (> 1 nmol L^{-1}) throughout the water column, thus suggesting analytical issues. However, these two stations were analysed twice and provided similar results, therefore discarding any analytical issues. This means that these high values originated either from genuine processes or from contamination issues. If there had been contamination issues, one would expect a more random distribution of DFe concentrations and less consistence throughout the water column. It thus appears that contamination issues were unlikely to happen. Similarly, the influence of water masses to explain these distributions was discarded as the observed high homogenized DFe concentrations were restricted to these two stations. Station 1, located at the continental shelf-break of the Iberian Margin, also showed enhanced PFe concentrations from lithogenic origin suggesting a margin source (Gourain et al., 2019). Conversely, no relationship was observed between DFe and PFe nor transmissometry for station 17. However, Ferron et al. (2016) reported a strong dissipation rate at the Azores-Biscay Rise (station 17) due to internal waves. The associated vertical energy fluxes could explain the homogenized profile of DFe at station 17, although such waves are not clearly evidenced in the velocity profiles. Consequently, the elevated DFe concentrations observed at station 17 remain unsolved.

4.2 DFe and hydrology keypoints

4.2.1 How do Air-sea interactions affect DFe concentration in the Irminger Sea?

Among the four distinct basins described in this paper, the Irminger Sea exhibited the highest DFe concentrations within the surface waters (from 0 to 250 m depth) with values ranging from 0.23 to 1.3 nmol L^{-1} for open-ocean stations. Conversely, low DFe concentrations were previously reported in the central Irminger Sea by Rijkenberg et al. (2014) (April-May, 2010) and Achterberg et al. (2018) (April-May and July-August, 2010) with DFe concentrations ranging from 0.11 to 0.15 and from ~ 0 to 0.14 nmol L^{-1}, respectively (see supplementary material Fig. S4 and Table S2). Differences might be due to the phytoplankton bloom advancement, the high remineralization rate (Lemaître et al., 2017) observed within the LSW in the Irminger Sea (see Section 4.1.3) and a deeper winter convection in early 2014. Indeed, enhanced surface DFe concentrations measured during GEOVIDE in the Irminger Sea could be due to intense wind forcing events that would deepen the winter Z_m down to the core of the Fe-rich LSW.

In the North Atlantic Ocean, the warm and salty water masses of the upper limb of the MOC are progressively cooled and become denser, and subduct into the abyssal ocean. In some areas of the SubPolar North Atlantic, deep convective winter mixing provides a rare connection between surface and deep waters of the MOC thus constituting an important mechanism in supplying nutrients to the surface ocean (de Jong et al., 2012; Louanchi and Najjar, 2001). Deep convective winter mixing is triggered by the effect of wind and a pre-conditioning of the ocean in such a way that the inherent stability of the ocean is minimal. Pickart et al. (2003) demonstrated that these conditions are satisfied in the Irminger Sea with the presence of weakly stratified surface water, a close cyclonic circulation, which leads to the shoaling of the thermocline and intense winter air-sea buoyancy fluxes (Marshall and Schott, 1999). Moore (2003) and Piron et al. (2016) described low-altitude westerly jets centred northeast of Cape Farewell, over the Irminger Sea, known as tip jet events. These events occur when wind is split around the orographic features of Cape Farewell, and are strong enough to induce deep convective mixing (Bacon et al., 2003; Pickart et al., 2003). It has also been shown that during winters with a positive North Atlantic Oscillation (NAO) index, the occurrence of such events is favoured (Moore, 2003; Pickart et al., 2003), which was the case in the winter 2013-2014, preceding the GEOVIDE voyage as opposed to previous studies (Lherminier, pers. comm.). The winter mixed layer depth prior to the cruise reached up to 1200 m depth in the Irminger Sea (Zunino et al., 2017), which was most likely attributed to a final deepening due to wind forcing events (centred at station 44). Such

505 winter entrainment was likely the process involved in the vertical supply of DFe within surface waters
506 fuelling the spring phytoplankton bloom with DFe values close to those found in LSW.
507
508 **4.2.2 Why don't we see a DFe signature in the Mediterranean Overflow Water (MOW)?**
509 On its northern shores, the Mediterranean Sea is bordered by industrialized European countries,
510 which act as a continuous source of anthropogenic derived constituents into the atmosphere, and on
511 the southern shores by the arid and desert regions of north African and Arabian Desert belts, which
512 act as sources of crustal material in the form of dust pulses (Chester et al., 1993; Guerzoni et al.,
513 1999; Martin et al., 1989). During the summer, when thermal stratification occurs, DFe concentrations
514 in the SML can increase over the whole Mediterranean Sea by 1.6-5.3 nmol L^{-1} in response to the
515 accumulation of atmospheric Fe from both anthropogenic and natural origins (Bonnet and Guieu,
516 2004; Guieu et al., 2010; Sarthou and Jeandel, 2001). After atmospheric deposition, the fate of Fe will
517 depend on the nature of aerosols, Fe-ligand binding capacity, vertical mixing, biological uptake, and
518 scavenging processes (Bonnet and Guieu, 2006; Wuttig et al., 2013). During GEOVIDE, MOW was
519 observed at percentages higher than ~ 60% from stations 1 to 13 between 900 and 1100 m depth and
520 associated with high dissolved aluminium (DAl, Menzel Barraqueta et al., 2018) concentrations (up to
521 38.7 nmol L^{-1}), confirming the high atmospheric deposition in the Mediterranean region. In contrast to
522 Al, no DFe signature was associated with MOW (Figs. 2 and 3). Using L-ADCP data during the cruise,
523 we estimated a translation velocity for the MOW of ~ 3-8 cm s-1, consistent with previous published
524 values (e.g. Armi et al., 1989; Schmidt et al., 1996). Our station 13 was located ~ 2000 km far from the
525 origin of the MOW, which would mean a transit time of ~ 1-2 years. This transit time would allow the
526 Fe signal to be preserved, when DFe residence times range from weeks to months in the surface
527 waters and from tens to hundreds of years in deep waters (de Baar and de Jong, 2001; Sarthou et al.,
528 2003; Croot et al., 2004; Bergquist and Boyle 2006; Gerringa et al 2015; Tagliabue et al., 2016). This
529 feature was also reported in some studies (Hatta et al., 2015; Thuróczy et al., 2010), while others
530 measured higher DFe concentrations in MOW (Gerringa et al., 2017; Sarthou et al., 2007). However,
531 MOW coincides with the maximum Apparent Oxygen Utilization (AOU) and it is not possible to
532 distinguish the MOW signal from the remineralisation signal (Sarthou et al., 2007). On the other hand,
533 differences between studies are likely originating from the intensity of atmospheric deposition and the
534 nature of aerosols. Indeed, Wagener et al. (2010) highlighted that large dust deposition events can
535 accelerate the export of Fe from the water column through scavenging. As a result, in seawater with

high DFe concentrations and where high dust deposition occurs, a strong individual dust deposition event could act as a sink for DFe. It thus becomes less evident to observe a systematic high DFe signature in MOW despite dust inputs.

4.2.3 Fe enrichment in Labrador Sea Water (LSW)

As described in Section 3.1, the LSW exhibited increasing DFe concentrations from its source area, the Labrador Sea, toward the other basins with the highest DFe concentrations observed within the Irminger Sea, suggesting that the water mass was enriched in DFe either locally in each basin or during its flow path (see supplementary material Fig. S3). These DFe sources could originate from a combination of high export of PFe and its remineralisation in the mesopelagic area and/or the dissolution of sediment.

The Irminger and Labrador Seas exhibited the highest averaged integrated TChl-a concentrations (98 ± 32 mg m^{-2} and 59 ± 42 mg m^{-2}) compared to the West European and Iceland Basins (39 ± 10 mg m^{-2} and 53 ± 16 mg m^{-2}), when the influence of margins was discarded. Stations located in the Irminger (stations 40-56) and Labrador (stations 63-77) Seas, were largely dominated by diatoms (>50% of phytoplankton abundances) and displayed the highest chlorophillide-*a* concentrations, a tracer of senescent diatom cells, likely reflecting post-bloom condition (Tonnard et al., in prep.). This is in line with the highest POC export data reported by Lemaitre et al. (2018) in these two oceanic basins. This likely suggests that biogenic PFe export was also higher in the Labrador and Irminger Seas than in the West European and Iceland Basins. In addition, Gourain et al. (2019) highlighted a higher biogenic contribution for particles located in the Irminger and Labrador Seas with relatively high PFe:PAl ratios (0.44 ± 0.12 mol:mol and 0.38 ± 0.10 mol:mol, respectively) compared to particles from the West European and Iceland Basins (0.22 ± 0.10 and 0.38 ± 0.14 mol:mol, respectively, see Fig. 6A in Gourain et al., 2019). However, they reported no difference in PFe concentrations between the four oceanic basins, when the influence of margins was discarded, which likely highlighted the remineralisation of PFe within the Irminger and Labrador Seas. Indeed, Lemaître et al. (2017) reported higher remineralisation rates within the Labrador (up to 13 mmol C m^{-2} d^{-1}) and Irminger Seas (up to 10 mmol C m^{-2} d^{-1}) using the excess barium proxy (Dehairs et al., 1997), compared to the West European and Iceland Basins (ranging from 4 to 6 mmol C m^{-2} d^{-1}). Therefore, the intense remineralisation rates measured in the Irminger and Labrador Seas likely resulted in enhanced DFe concentrations within LSW.

Higher DFe concentrations were, however, measured in the Irminger Sea compared to the Labrador Sea and coincided with lower transmissometry values (i.e. 98.0-98.5% vs. >99%), thus suggesting a particle load of the LSW. This could be explained by the reductive dissolution of Newfoundland Margin sediments. Indeed, Lambelet et al. (2016) reported high dissolved neodymium (Nd) concentrations (up to 18.5 pmol.kg^{-1}) within the LSW at the edge of the Newfoundland Margin (45.73°W, 51.82°N) as well as slightly lower Nd isotopic ratio values relative to those observed in the Irminger Sea. They suggested that this water mass had been in contact with sediments approximately within the last 30 years (Charette et al., 2015). Similarly, during GA03, Hatta et al. (2015) attributed the high DFe concentrations in the LSW to continental margin sediments. Consequently, it is also possible that the elevated DFe concentrations from the three LSW branches which entered the West European and Iceland Basins and Irminger Sea was supplied through sediment dissolution (Measures et al., 2013) along the LSW pathway.

The enhanced DFe concentrations measured in the Irminger Sea and within the LSW were thus likely attributed to the combination of higher productivity, POC export and remineralisation as well as a DFe supply from reductive dissolution of Newfoundland sediments to the LSW along its flow path. Using temperature and salinity anomalies, Yashayaev et al. (2007) showed that the LSW reached the Irminger Sea and the Iceland Basin in 1-2 years and 4-5 years, respectively, after its formation in the Labrador Sea. The LSW transit time in this region is thus compatible with a DFe residence times (see above).

4.2.4 Enhanced DFe concentrations in the Irminger Sea bottom water

Bottom waters from the Irminger Sea exhibited the highest DFe concentrations from the whole section, excluding the stations at the margins. Such a feature could be due to i) vertical diffusion from local sediment, ii) lateral advection of water mass(es) displaying enhanced DFe concentrations, and iii) local dissolution of Fe from particles. Hereafter, we discuss the plausibility of these three hypotheses.

The GEOTRACES GA02 voyage (leg 1, 64PE319) which occurred in April-May 2010 from Iceland to Bermuda sampled two stations north and south of our station 44 (~ 38.95°W, 59.62°N): station 5 (~ 37.91°W, 60.43°N) and 6 (~ 39.71°W, 58.60°N), respectively. High DFe concentrations in samples collected close to the bottom were also observed and attributed to sediment inputs highlighting boundary exchange between seawater and surface sediment (Lambelet et al., 2016; Rijkenberg et al., 2014). However, because a decrease in DFe concentrations was observed at our station 44 from 2500 m depth down to the bottom (Fig. 3 and Table S1), it appeared to be unlikely that these high DFe

concentrations will be the result of local sediment inputs, as no DFe gradient from the deepest samples to those above was observed.

Looking at salinity versus depth for these three stations, one can observe the intrusion of Polar Intermediate Water (PIW) at station 44 during GEOVIDE, which was not observed during the GA02 voyage and which contributed to about 14% of the water mass composition (García-Ibáñez et al., 2018) and might therefore be responsible for the high DFe concentrations (see supplementary material Fig. S5A). On the other hand, the PIW was also observed at station 49 (from 390 to 1240 m depth), 60 (from 440 to 1290 m depth), 63 (from 20 to 1540 m depth), 68 (3340 m depth), 69 (from 3200 to 3440 m depth), 71 (from 2950 to 3440 m depth) and 77 (60 and 2500 m depth) with similar or higher contributions of the PIW without such high DFe concentrations (maximum DFe = 1.3 ± 0.1 nmol L^{-1}, 1240 m depth at station 49). At this station, the DSOW relative abundance was more than 20% (Supp. Fig. S5). The overflow of this dense water in the Irminger Sea is associated with intense cyclonic boluses (Käse et al. 2003) and the entrainment of waters from the Greenland margin and slope by pulses of DSOW occurs all along its transport from Denmark Strait to the Greenland tip (Magaldi et al., 2011; von Appen et al., 2014). This phenomenon may enrich the DSOW with Fe as well as other elements. This was also observed for radium and actinium with a deviation from the conservative behaviour of 226Ra (Le Roy et al., 2018) and an increase of 227Ac activity at station 44 at 2500 m, reflecting inputs of these tracers. Therefore, the high DFe concentrations observed in the Irminger Sea might be inferred from substantial load of Fe-rich particles when DSOW is in contact with the Greenland margin.

4.2.5 Reykjanes Ridge: Hydrothermal inputs or Fe-rich seawater?

Hydrothermal activity was assessed over the Mid Atlantic Ridge, namely the Reykjanes Ridge (RR), from stations 36 to 40. Indeed, within the interridge database (http://www.interridge.org), the Reykjanes Ridge is reported to have active hydrothermal sites. The sites were either confirmed (Baker and German, 2004; German et al., 1994; Olaffson et al., 1991; Palmer et al., 1995) close to Iceland or inferred (e.g. Chen, 2003; Crane et al., 1997; German et al., 1994; Sinha et al., 1997; Smallwood and White, 1998) closer to the GEOVIDE section as no plume was detected but a high backscatter was reported potentially corresponding to a lava flow. Therefore, hydrothermal activity at the sampling sites remains unclear with no elevated DFe concentrations nor temperature anomaly above the ridge (station 38). However, enhanced DFe concentrations (up to 1.5 ± 0.22 nmol L^{-1}, station 36, 2200 m

depth) were measured east of the Reykjanes Ridge (Fig. 3). This could be due to hydrothermal activity and resuspension of sunken particles at sites located North of the section and transported through ISOW towards the section (Fig. 3). Indeed, Achterberg et al. (2018) highlighted at ~60°N and over the Reykjanes Ridge a southward lateral transport of an Fe plume of up to 250-300 km. In agreement with these observations, previous studies (e.g. Fagel et al., 1996; Fagel et al., 2001; Lackschewitz et al., 1996; Parra et al., 1985) reported marine sediment mineral clays in the Iceland Basin largely dominated by smectite (> 60%), a tracer of hydrothermal alteration of basaltic volcanic materials (Fagel et al., 2001; Tréguer and De La Rocha, 2013). Kanzow and Zenk (2014) investigated the fluctuations of the ISOW plume around RR. The transit time, west of RR, between 60°N and the Bight Fracture Zone (BFZ) was around 5 months, compatible with the residence time of DFe (see above). Hence, the high DFe concentrations measured east of RR could be due to a hydrothermal source and/or the resuspension of (basaltic) particles and their subsequent dissolution.

West of the Reykjanes Ridge, a DFe-enrichment was also observed in ISOW at station 40 within the Irminger Sea (Fig. 3). The low transmissometer values within ISOW in the Irminger Sea (station 44) compared to the Iceland Basin (station 32) suggested a higher particle load (Fig. 4A in Gourain et al., 2019). These particles could come from the Bight Fracture Zone (BFZ, 56.91°N and 32.74°W) (Fig. 1) (Lackschewitz et al., 1996; Zou et al., 2017) since the transit time of the ISOW between BFZ and our station 40 is around 3 months (Kanzow and Zenk, 2014)..

4.3 What are the main sources of DFe in surface waters?

During GEOVIDE, enhanced DFe surface concentrations were observed at several stations (stations 1-4, 53, 61, 78) highlighting an external source of Fe to surface waters. The main sources able to deliver DFe to surface waters are riverine inputs, glacial inputs and atmospheric deposition. In the following sections, these potential sources of DFe to surface waters will be discussed.

4.3.1 Tagus riverine inputs

Enhanced DFe surface concentrations (up to 1.07 ± 0.12 nmol L^{-1}) were measured over the Iberian Margin (stations 1-4) and coincided with salinity minima (~ <35) and enhanced DAl concentrations (up to 31.8 nmol L^{-1}, Menzel Barraqueta et al., 2018). DFe and DAl concentrations were both significantly negatively correlated with salinity (R^2 = ~1 and 0.94, respectively) from stations 1 to 13 (Fig. 5).

Salinity profiles from station 1 to 4 showed evidence of a freshwater source with surface salinity ranging from 34.95 (station 1) to 35.03 (station 4). Within this area, only two freshwater sources were possible: 1) wet atmospheric deposition (4 rain events, Shelley, pers. comm.) and 2) the Tagus River, since the ship SADCP data revealed a northward circulation with a velocity of around 0.1 m/s (P. Lherminier and P. Zunino, Ifremer Brest, pers. comm.). The transit time from the estuary to our stations above the shelf is around 15 days (150 km), which is short enough to preserve the DFe signal. Our SML DFe inventories were about three times higher at station 1 (~ 1 nmol L^{-1}) than those calculated during the GA03 voyage (~ 0.3 nmol L^{-1}, station 1). Atmospheric deposition were about one order of magnitude higher during GA03 than during GA01 (Shelley et al., 2018; Shelley et al., 2015), thus the atmospheric source seemed to be minor during GA01. Consequently, the Tagus River appears as the most likely source responsible for these enhanced DFe concentrations, either as direct input of DFe or indirectly through Fe-rich sediment carried by the Tagus River and their subsequent dissolution. The Tagus estuary is the largest in the western European coast and very industrialized (Canário et al., 2003; de Barros, 1986; Figueres et al., 1985; Gaudencio et al., 1991; Mil-Homens et al., 2009), that extends through an area of 320 km^2 and is characterized by a large water flow of 15.5 10^9 m^3 y^{-1} (Fiuza, 1984). Many types of industry (e.g. heavy metallurgy, ore processing, chemical industry) release metals including Fe, which therefore result in high levels recorded in surface sediments, suspended particulate matter, water and organisms in the lower estuary (Santos-Echeandia et al., 2010).

4.3.2 High latitude meteoric water and sea-ice processes

Potential sources of Fe at stations 53, 61 and 78 include meteoric water (MW, referring to precipitation, runoff and continental glacial melt), sea-ice melt (SIM), seawater interaction with shallow sediments and advection of water transported from the Arctic sourced by the Fe-rich TransPolar Drift (TPD, Klunder et al. (2012); see supplementary material Fig. S4 and Table S2). The vertical profiles of both potential temperature and salinity in the Greenland and Newfoundland Margins (station 53, 61 and 78, Fig. 4 D, E, and F) highlighted the presence of this freshwater lens likely originating from the Arctic Ocean. They were present in the upper 60 m (station 53) and and 40 m (stations 61 and 78) depth. The most plausible source of this freshwater lens would be meteoric water and sea-ice melting. Deeper in the water column, net brine release (defined as a negative value of sea-ice melting) were observed at stations 53 (below 40 m depth, Fig. 4D) 61 (in the whole water column, Fig. 4E) and 78

690 (below 30 m depth, Fig. 4F). The release of brines could originate from two different processes: the
691 sea-ice formation or the early melting of multiyear sea ice due to gravitational drainage and
692 subsequent brine release (Petrich and Eicken, 2010; Wadhams, 2000). Indeed, during the winter
693 preceding the GEOVIDE voyage, multiyear sea ice extended 200 km off the Greenland stations
694 (http://nsidc.org/arcticseaicenews/). In the following sections, we discuss the potential for meteoric
695 water supply, sea-ice formation and sea-ice melting to affect DFe distribution.
696
697 *4.3.2.1 The Greenland shelf*
698 Considering the sampling period at stations 53 (16 June 2014) and 61 (19 June 2014), sea-ice
699 formation is unlikely to happen as this period coincides with summer melting in both the Central Arctic
700 and East Greenland (Markus et al., 2009). However, it is possible that the brines observed in our study
701 could originates from sea-ice formation which occurred during the previous winter(s) at 66°N (and/or
702 higher latitudes). The brine signalat station 61 between 40 and 140 m was associated with a depletion
703 in both DFe and PFe, which may be attributed to sea ice formation processes. Indeed, as soon as sea
704 ice forms, sea salts are efficiently flushed out of the ice while PFe is trapped within the crystal matrix
705 and DFe accumulates, leading to an enrichment factor of these two Fe fractions compared to
706 underlying seawater (Janssens et al., 2016). Conversely, the strongest brine signal observed at
707 station 53 (between 50 and 160 m) showed slight enrichments in both DFe and PFe, which may be
708 attributed to sea ice melting and the associated release into the underlying water column.
709 Surface waters at stations 53 and 61 were characterized by high MW fractions together with
710 enrichments in PFe at station 53 and in both DFe and PFe at station 61 (Fig. 4D and E). These results
711 are in line with previous observations, which highlighted strong inputs of DFe from a meteoric water
712 melting source in Antarctica (Annett et al., 2015). At station 61, the relative depletion of DFe at 30 m
713 compared to 50 m may be due to phytoplankton uptake, as indicated by the high TChl-*a*
714 concentrations (up to 6.6 mg m^{-3}, Fig. 4D). Hence, it seemed that meteoric water inputs from the
715 Greenland Margin likely fertilized surface waters with DFe, enabling the phytoplankton bloom to
716 subsist.
717
718 *4.3.2.2 The Newfoundland shelf*
719 Newfoundland shelf waters (station 78) were characterized by high MW fractions (up to 7%),
720 decreasing from surface to 200 m depth (~2%). These waters were associated with a net sea-ice

721 melting signal from the near surface to ~10 m depth followed by a brine release signal down to 200 m
722 depth with the maximum contribution measured at ~30 m depth. Within the surface waters (above 20
723 m depth), no elevation in DFe, DAl nor PFe was noticed despite the low measured TChl-*a*
724 concentrations (TChl-*a* ~ 0.20 mg m^{-3}). This suggests that none of these inputs (sea-ice melting and
725 meteoric water) were able to deliver DFe or that these inputs were minor compared to sediment inputs
726 from the Newfoundland Margin. Surprisingly, the highest TChl-*a* biomass (TChl-*a* > 9 mg m^{-3}) from the
727 whole section was measured at 30 m depth corresponding to the strongest brine release signal. This
728 either suggests that the brine likely contained important amounts of Fe (dissolved and/or particulate
729 Fe) that were readily available for phytoplankton and consumed at the sampling period by potentially
730 sea-ice algae themselves (Riebesell et al., 1991) or that another nutrient was triggering the
731 phytoplankton bloom.
732
733 **4.3.3 Atmospheric deposition**
734 On a regional scale, the North Atlantic basin receives the largest amount of atmospheric inputs due to
735 its proximity to the Saharan Desert (Jickells et al., 2005), yet even in this region of high atmospheric
736 deposition, inputs are not evenly distributed. Indeed, aerosol Fe loading measured during GEOVIDE
737 (Shelley et al., 2017) were much lower (up to four orders of magnitude) than those measured during
738 studies from lower latitudes in the North Atlantic (e.g. Baker et al., 2013; Buck et al., 2010; and for
739 GA03, Shelley et al., 2015), but atmospheric inputs could still be an important source of Fe to surface
740 waters in areas far from land.
741 In an attempt to estimate whether there was enough atmospheric input to sustain the SML DFe
742 concentrations, we calculated Turnover Times relative to Atmospheric Deposition (TTADs, Guieu et
743 al., 2014). To do so, we made the following assumptions: 1) the aerosol concentrations are a snapshot
744 in time but are representative of the study region, 2) the aerosol solubility estimates based on two
745 sequential leaches are an upper limit of the aerosol Fe in seawater and 3) the water column stratified
746 just before the deposition of atmospheric inputs, so MLD DFe will reflect inputs from above. Thus, the
747 TTADs were defined as the integrated DFe concentrations in the SML for each station divided by the
748 contribution of soluble Fe contained in aerosols averaged per basin to the water volume of the SML.
749 Although, TTADs were lower in the West European and Iceland Basins with an average of ~ 9 ± 3
750 months compared to other basins (7 ± 2 years and 5 ± 2 years for the Irminger and Labrador Seas,
751 respectively) (Fig. 6) they were about three times higher than those reported for areas impacted by

Saharan dust inputs (~ 3 months, Guieu et al., 2014). Therefore, the high TTADs measured in the Irminger and Labrador Seas and ranging from 2 to 15 years provided further evidence that atmospheric deposition were unlikely to supply Fe in sufficient quantity to be the main source of DFe (see Sections 4.2.1 and 4.3.2) while in the West European and Iceland Basins they played an additional source, perhaps the main source of Fe especially at station 36 which displayed TTAD of 3 months.

4.3.4 Sediment input

4.3.4.1 Margins:

DFe concentration profiles from all coastal stations (stations 2, 4, 53, 56, 61 and 78) are reported in Figure 4. To avoid surface processes, only depths below 100 m depth will be considered in the following discussion. DFe and PFe followed a similar pattern at stations 2, 53, 56, and 78 with increasing concentrations towards the sediment, suggesting that either the sources of Fe supplied both Fe fractions (dissolved and particulate) or that PFe dissolution from sediments supplied DFe. Among the different margins, the Newfoundland Margin exhibited the highest deep-water DFe and PFe concentrations. Conversely, stations 4 and 61 exhibited a decrease in DFe concentrations in the samples closest to the seafloor whereas PFe increased. DFe:PFe ratios ranged from 0.01 (station 2, bottom sample) to 0.27 (station 4, ~ 400 m depth) mol:mol with an average value of 0.11 ± 0.07 mol:mol (n = 23, Table 3). This could be explained by the different nature of the sediments and/or different sediment conditions (e.g. redox, organic content). Based on particulate and dissolved Fe and dissolved Al data (Gourain et al., 2019; Menzel Barraqueta et al., 2018, Table 3), three main different types of margins were reported (Gourain et al., 2019) with the highest lithogenic contribution observed at the Iberian Margin (stations 2 and 4) and the highest biogenic contribution at the Newfoundland Margin (station 78). These observations are consistent with higher TChl-*a* concentrations measured at the Newfoundland Margin and to a lesser extent at the Greenland Margin and the predominance of diatoms relative to other functional phytoplankton classes at both margins (Tonnard et al., in prep.). To sum up, the more biogenic sediments (Newfoundland Margin) were able to mobilise more Fe in the dissolved phase than the more lithogenic sediments (Iberian Margin), in agreement with Boyd et al. (2010) who reported greater remineralization of PFe from biogenic PFe than from lithogenic PFe based on field experiment and modelling simulations.

4.3.4.2 Nepheloid layers:

Samples associated with high levels of particles (transmissometer < 99%) and below 500 m depth displayed a huge variability in DFe concentrations. From the entire dataset, 63 samples (~13% of the entire dataset) followed this criterion with 14 samples from the West European Basin (station 1), 4 samples from the Iceland Basin (stations 29, 32, 36 and 38), 43 samples from the Irminger Sea (stations 40, 42, 44, 49 and 60) and 2 samples from the Labrador Sea (station 69). To determine which parameter was susceptible to explain the variation in DFe concentrations in these nepheloid layers, a Principal Component Analysis (PCA) on these samples. The input variables of the PCA were particulate Fe, Al, and particulate manganese (PMn) (Gourain et al., 2019), DAl (Menzel Barraqueta et al., 2018) and Apparent Oxygen Utilization (AOU) and were all correlated to DFe concentrations explaining all together 93% of the subset variance (see supplementary material Fig. S6). The first dimension of the PCA was represented by PAl, PFe and PMn concentrations and explained 59.5% of the variance, while the second dimension was represented by the DAl and the AOU parameters, explaining 33.2% of the variance. The two sets of variables were nearly at right angle from each other, indicating no correlation between them.

The variations in DFe concentrations measured in bottom samples from stations 32, 36 (Iceland Basin), 42 and 44 (Irminger Sea) and 69 (Labrador Sea) were mainly explained by the first dimension of the PCA (see supplementary material Fig. S6). Therefore, samples characterized by the lowest DFe concentrations (stations 32 and 69) were driven by particulate Al and Mn concentrations and resulted in an enrichment of Fe in the particulate phase. These results are in agreement with previous studies showing that the presence of Mn within particles can induce the formation of Fe-Mn oxides, contributing to the removal of Fe and Mn from the dissolved phase (Kan et al., 2012; Teng et al., 2001).

Low DFe concentrations (bottom samples from stations 42 and 1) were linked to DAl inputs and associated with lower AOU values. The release of Al has previously been observed from Fe and Mn oxide coatings on resuspended sediments under mildly reducing conditions (Van Beusekom, 1988). Conversely, higher DFe concentrations were observed for stations 44 and 49 and to a lesser extent station 60 coinciding with low DAl inputs and higher oxygen levels. This observation challenges the traditional view of Fe oxidation with oxygen, either abiotically or microbially induced. Indeed, remineralisation can decrease sediment oxygen concentrations, promoting reductive dissolution of PFe oxyhydroxides to DFe that can then diffuse across the sediment water interface as DFe(II)

colloids (Homoky et al., 2011). Such processes will inevitably lead to rapid Fe removal through precipitation of nanoparticulate or colloidal Fe (oxyhydr)oxides, followed by aggregation or scavenging by larger particles (Boyd and Ellwood, 2010; Lohan and Bruland, 2008) unless complexion with Fe-binding organic ligands occurs (Batchelli et al., 2010; Gerringa et al., 2008). There exist, however, another process that is favoured in oxic benthic boundary layers (BBL) with low organic matter degradation and/or low Fe oxides, which implies the dissolution of particles after resuspension, namely the non-reductive dissolution of sediment (Homoky et al., 2013; Radic et al., 2011). In addition, these higher oxygenated samples were located within DSOW, which mainly originate (75% of the overflow) from the Nordic Seas and the Arctic Ocean (Tanhua et al., 2005), in which the ultimate source of Fe was reported by Klunder et al. (2012) to come from Eurasian river waters. The major Arctic rivers were highlighted by Slagter et al. (2017) to be a source of Fe-binding organic ligands that are then further transported via the TPD across the Denmark Strait. Hence, the enhanced DFe concentrations measured within DSOW might result from Fe-binding organic ligand complexation that were transported to the deep ocean as DSOW formed rather than the non-reductive dissolution of sediment.

4.4 How does biological activity modify DFe distribution?

Overall, almost all the stations from the GEOVIDE voyage displayed DFe minima in surface water associated with some maxima of TChl-*a* (see supplementary material Fig. S1). In the following section, we specifically address the question of whether DFe concentrations potentially limit phytoplankton growth. Note that macronutrients and DFe limitations relative to phytoplankton functional classes are dealt with Tonnard et al. (in prep.).

A key determinant for assessing the significance of a DFe source is the magnitude of the DFe:macronutrient ratio supplied, since this term determines to which extent DFe will be utilised. The DFe:NO_3^- ratios in surface waters varied from 0.02 (station 36) to 38.6 (station 61) mmol:mol with an average of 5 ± 10 mmol:mol (see supplementary material Fig. S7). Values were typically equal or lower than 0.28 mmol mol^{-1} in all basins except at the margins and at stations 11, 13, 68, 69 and 77. The low nitrate concentrations observed at the eastern and western Greenland and Newfoundland Margins reflected a strong phytoplankton bloom which had reduced the concentrations as highlighted by the elevated integrated TChl-*a* concentrations ranging from 129.6 (station 78) to 398.3 (station 61) mg m^{-2}. At the Iberian Margin, they likely reflected the influence of the N-limited Tagus River (stations

1, 2 and 4) with its low TChl-*a* integrated concentrations that ranged from 31.2 (station 1) to 46.4 (station 4) mg m^{-2}. The high DFe:NO_3^- ratios determined at those stations, which varied from 13.4 (station 78) to 38.6 (station 61) mmol:mol, suggested that waters from these areas, despite having the lowest NO_3^- concentrations, were relatively enriched in DFe compared to waters from the Iceland Basin and the Irminger Sea.

In our study, DFe:NO_3^- ratios displayed a gradient from the West European Basin to Greenland (supplementary material S7 and S8). This trend only reverses when the influence of Greenland was encountered, as also observed by Painter et al. (2014). The remineralisation of organic matter is a major source of macro and micronutrients in subsurface waters (from 50 to 250 m depth). Remineralisation is associated with the consumption of oxygen and therefore, Apparent Oxygen Utilization (AOU) can provide a quantitative estimate of the amount of material that has been remineralised. While no relationship was observed below 50 m depth for NO_3^- or DFe and AOU considering all the stations, a significant correlation was found in the Subpolar gyre when removing the influence of margins (stations 29-49, 56, 60, 63-77) (AOU = 3.65 NO_3^- – 21.85, R^2=0.70, n=50, p-value < 0.001). This correlation indicates that remineralisation of Particulate Organic Nitrogen (PON) greatly translates into Dissolved Inorganic Nitrogen (DIN) and that NO_3^- can be used as a good tracer for remineralisation in the studied area. Within these Subpolar gyre waters, there was a significant correlation between DFe and AOU (AOU = 23.92 DFe + 10.45, R^2=0.37, n=58, p-value < 0.001). The open-ocean stations from the subpolar gyre also exhibited a good linear correlation between DFe and NO_3^- DFe = 0.08 NO3- - 0.48, R^2=0.45, n=50, p-value < 0.05).(see supplementary material Fig. S8). The negative intercept of the regression line reflects possible excess of preformed NO_3^- compared to DFe in these water masses. These significant correlations allow us to use the Fe* tracer to assess where DFe concentrations potentially limit phytoplankton growth by subtracting the contribution of organic matter remineralisation from the dissolved Fe pool, as defined by Rijkenberg et al. (2014) and Parekh et al. (2005) for PO_4^{3-}, and modified here for NO_3^- as follows:

(eq. 5)

where $R_{Fe:N}$ refers to the average biological uptake ratio Fe over nitrogen, and [NO_3^-] refers to nitrate concentrations in seawater. Although, we imposed a fixed biological $R_{Fe:N}$ of 0.05 mmol mol^{-1}, it is important to note that the biological uptake ratio of DFe:NO_3^- is not likely to be constant. Indeed, this ratio has been found to range from 0.05 to 0.9 mmol mol^{-1} depending on species (Ho et al., 2003; Sunda and Huntsman, 1995; Twining et al., 2004). The ratio we choose is thus less drastic to assess

potential Fe limitation and more representative of the average biological uptake of DFe over NO_3^- calculated for this study (i.e. $R_{Fe:N}$ = 0.08 ± 0.01 mmol mol^{-1}, for Subpolar waters). Negative values of Fe* indicate the removal of DFe that is faster than the input through remineralisation or external sources and positive values suggest input of DFe from external sources (Fig. 7). Consequently, figure 7 shows that phytoplankton communities with very high Fe requirements relative to NO_3^- ($R_{Fe:N}$ = 0.9 mmol mol^{-1}) will only be able to grow above continental shelves where there is a high supply of DFe as previously reported by Nielsdóttir et al. (2009) and Painter et al. (2014). All these results are corroborating the importance of the Tagus River (Iberian Margin, see section 4.2.1), glacial inputs in the Greenland and Newfoundland Margins (see section 4.2.2) and to a lesser extent atmospheric inputs (see section 4.2.3) in supplying Fe with Fe:N ratios higher than the average biological uptake/demand ratio. Figure 7 (see also supplementary material S7, S9, S10 and S11) exhibits Fe:N ratios lower than 0.05 mmol mol^{-1}, suggesting that Fe could also limit the low–Fe requirement phytoplankton class ($R_{Fe:N}$ = 0.05 mmol mol^{-1}) within the Iceland Basin, the Irminger, and the Labrador Seas. The Fe deficiency observed in surface waters (> 50 m depth) from the Irminger and the Labrador Seas might be explained by low atmospheric deposition to IcSPMW and LSW (Shelley et al., 2017). Low atmospheric Fe supply and sub-optimal Fe:N ratios in winter overturned deep water could favour the formation of the High-Nutrient, Low-Chlorophyll (HNLC) conditions. The West European Basin, despite exhibiting some of the highest DFe:NO_3^- ratios within surface waters, displayed one of the strongest Fe-depletions from 50 m depth down to the bottom (see supplementary material Fig. S9 and S10), suggesting that the main source of Fe was coming from dust deposition and/or riverine inputs.

Similarly as for the West European Basin, the pattern displayed in the surface map of DFe:NO_3^- ratios (supplementary material S9) extended to about 50 m depth, after which the trend reversed (Fig. 7 and supplementary material Fig. S7). Below 50 m depth, the Fe* tracer (Fig. 7) was positive in the Irminger Sea and overall negative in the other basins. In the Irminger Sea positive Fe* values were likely the result of the winter entrainment of Fe-rich LSW (see section 4.2.1) coinciding with high remineralised carbon fluxes in this area (station 44; Lemaître et al., 2017) (see section 4.2.2). The largest drawdown in DFe:NO_3^- ratios was observed between stations 34 and 38 and was likely due to the intrusion of IcSPMW, this water mass exhibiting low DFe and high in NO_3^- (from 7 to 8 µmol L^{-1}) concentrations. Similarly, SAIW exhibited high NO_3^- concentrations. Both the IcSPMW and the SAIW sourced from the NAC. The NAC as it flows along the coast of North America receives atmospheric depositions from

anthropogenic sources (Shelley et al., 2017; 2015) which deliver high N relative to Fe (Jickells and Moore, 2015) and might be responsible for the observed ranges.

5 Conclusion

The DFe concentrations measured during this study were in good agreement with previous studies that spanned the West European Basin. However, within the Irminger Basin the DFe concentrations measured during this study were up to 3 times higher than those measured by Rijkenberg et al. (2014) in deep waters (> 1000 m depth). This is likely explained by the different water masses encountered (i.e. the Polar Intermediate Water, ~ 2800 m depth) and by a stronger signal of the Iceland Scotland Overflow Water (ISOW) from 1200 to 2300 m depth. This corresponded to the most striking feature of the whole section with DFe concentrations reaching up to 2.5 nmol L^{-1} within ISOW, Denmark Strait Overflow Water (DSOW) and Labrador Sea Water (LSW), three water masses that are part of the Deep Western Boundary Current and was likely the result of a lateral advection of particles in the Irminger Sea. However, as these water masses reached the Labrador Sea, lower DFe levels were measured. These differences could be explained by different processes occurring within the benthic nepheloid layers, where DFe was sometimes trapped onto particles due to Mn-sediment within the Labrador Sea (Gourain et al., 2019) and sometimes released from the sediment potentially as a result of interactions with dissolved organic matter. Such Fe-binding organic ligands could have also been produced locally due to the intense remineralisation rate reported by Lemaître et al. (2017) of biogenic particles (Boyd et al., 2010; Gourain et al., 2019). The LSW exhibited increasing DFe concentrations along its flow path, likely resulting from sediment inputs at the Newfoundland Margin. Although DFe inputs through hydrothermal activity were expected at the slow spreading Reykjanes Ridge (Baker and German, 2004; German et al., 1994), our data did not provide evidence of this specific source as previously suggested by Achterberg et al. (2018) at ~60°N.

In surface waters several sources of DFe were highlighted especially close to land, with riverine inputs from the Tagus River at the Iberian margin (Menzel Barraqueta et al., 2018) and meteoric inputs (including coastal runoff and glacial meltwater) at the Newfoundland and the Greenland margins (Benetti et al., 2016). Substantial sediment input was observed at all margins but with varying intensity. The highest DFe sediment input was located at the Newfoundland margin, while the lowest was observed at the eastern Greenland margin. These differences could be explained by the different nature of particles with the most lithogenic located at the Iberian margin and the most biogenic, at the

Newfoundland margin (Gourain et al., 2019). Although previous studies (e.g. Jickells et al., 2005; Shelley et al., 2015) reported that atmospheric inputs substantially fertilized surface waters from the West European Basin, in our study, only stations located in the West European and Iceland Basins exhibited enhanced SML DFe inventories with lower TTADs. However, these TTADs were about three times higher than those reported for Saharan dust inputs and thus atmospheric deposition appeared to be a minor source of Fe during the sampling period. Finally, there was evidence of convective inputs of the LSW to surface seawater caused by long tip jet events (Piron et al., 2016) that deepened the winter mixed layer down to ~ 1200 m depth (Zunino et al., 2017), in which Fe was in excess of nitrate and therefore, Fe was not limiting.

Acknowledgements

We are greatly indebted to the master, Gilles Ferrand, the officers and crew from the N/O *Pourquoi Pas?* for their logistic support during the GEOVIDE voyage. We would like to give a special thanks to Pierre Branellec, Michel Hamon, Catherine Kermabon, Philippe Le Bot, Stéphane Leizour, Olivier Ménage (Laboratoire d'Océanographie Physique et Spatiale), Fabien Pérault and Emmanuel de Saint Léger (Division Technique de l'INSU, Plouzané, France) for their technical expertise during clean CTD deployments as well as Emilie Grosteffan and Manon Le Goff for the analysis of nutrients. We also wanted to thank the Pôle Spectrométrie Océan (PSO, Plouzané, France) for letting us use the Element XR HR-ICP-MS. Greg Cutter is also strongly acknowledged for his help in setting up the new French clean sampling system. Catherine Schmechtig is thanked for the LEFE-CYBER database management. This work was funded by the French National Research Agency ANR GEOVIDE (ANR-13-BS06-0014) and RPDOC BITMAP (ANR-12-PDOC-0025-01), the French National Center for Scientific Research (CNRS-LEFE-CYBER), the LabexMER (ANR-10-LABX-19) and Ifremer and was supported for the logistic by DT-INSU and GENAVIR. Manon Tonnard was supported by a cotutelle joint PhD scholarship from the Université de Bretagne Occidentale (UBO-IUEM) and the University of Tasmania (UTAS-IMAS).

All dissolved iron (DFe) data are available in the supplementary material S1.

967 **References**

968 Achterberg, E. P., Steigenberger, S., Marsay, C. M., LeMoigne, F. A., Painter, S. C., Baker, A. R.,
969 Connelly, D. P., Moore, C. M., Tagliabue, A., and Tanhua, T.: Iron Biogeochemistry in the High
970 Latitude North Atlantic Ocean, Scientific reports, 8, 1-15, 10.1038/s41598-018-19472-1, 2018.
971 Aminot, A., and Kerouel, R.: Dosage automatique des nutriments dans les eaux marines, Quae ed.,
972 2007.
973 Annett, A. L., Skiba, M., Henley, S. F., Venables, H. J., Meredith, M. P., Statham, P. J., and
974 Ganeshram, R. S.: Comparative roles of upwelling and glacial iron sources in Ryder Bay, coastal
975 western Antarctic Peninsula, Marine Chemistry, 176, 21-33, 10.1016/j.marchem.2015.06.017,
976 2015.
977 Armi, L., Hebert, D., Oakey, N., Price, J., Richardson, P. L., Rossby, T. and Ruddick, B.: The history
978 and decay of a Mediterranean salt lens, Nature, 333(6174), 649–651, doi:10.1038/333649a0,
979 1988.
980 Bacon, S., Gould, W. J., and Jia, Y.: Open-ocean convection in the Irminger Sea, Geophysical
981 Research Letters, 30, 1246, doi:10.1029/2002GL016271, 2003.
982 Baker, A. R., Adams, C., Bell, T. G., Jickells, T. D., and Ganzeveld, L.: Estimation of atmospheric
983 nutrient inputs to the Atlantic Ocean from 50°N to 50°S based on large-scale field sampling: Iron
984 and other dust-associated elements, Global Biogeochemical Cycles, 27, 755-767,
985 10.1002/gbc.20062, 2013.
986 Baker, A. T., and German, C. R.: On the Global Distribution of Hydrothermal vent Fields, . In Mid-
987 Ocean Ridges: Hydrothermal Interactions Between the Lithosphere and Oceans, Geophysical
988 Monograph Series 148, C.R. German, J. Lin, and L.M. Parson (eds.), 245–266 (2004)
989
990 Barton, A. D., Greene, C. H., Monger, B. C., and Pershing, A. J.: The Continuous Plankton Recorder
991 survey and the North Atlantic Oscillation: Interannual- to Multidecadal-scale patterns of
992 phytoplankton variability in the North Atlantic Ocean, Progress in Oceanography, 58, 337-358,
993 10.1016/j.pocean.2003.08.012, 2003.
994 Batchelli, S., Muller, F. L. L., Chang, K. C., and Lee, C. L.: Evidence for Strong but Dynamic Iron-
995 Humic Colloidal Associations in Humic-Rich Coastal Waters., Environmental Science &
996 Technology, 44, 8485-8490, https://doi.org/10.1021/es101081c, 2010.

997 Benetti, M., Reverdin, G., Pierre, C., Khatiwala, S., Tournadre, B., Olafsdottir, S., and Naamar, A.:
998 Variability of sea ice melt and meteoric water input in the surface Labrador Current off
999 Newfoundland, Journal of Geophysical Research Oceans, 121, 2841-2855,
1000 doi:10.1002/2015JC011302., 2016.
1001 Benetti, M., Reverdin, G., Lique, C., Yashayaev, I., Holliday, N. P., Tynan, E., Torres-Valdes, S.,
1002 Lherminier, P., Tréguer, P., and Sarthou, G.: Composition of freshwater in the spring of 2014 on
1003 the southern Labrador shelf and slope, Journal of Geophysical Research: Oceans, 122, 1102-
1004 1121, 10.1002/2016jc012244, 2017.
1005 Bergquist, B. A. and Boyle, E. A.: Dissolved iron in the tropical and subtropical Atlantic Ocean, Global
1006 Biogeochemical Cycles, 20(1), doi:10.1029/2005GB002505, 2006.
1007 Bersch, M., Yashayaev, I., and Koltermann, K. P.: Recent changes of the thermohaline circulation in
1008 the subpolar North Atlantic, Ocean Dynamics, 57, 223-235, 10.1007/s10236-007-0104-7, 2007.
1009 Bhatia, M. P., Kujawinski, E. B., Das, S. B., Breier, C. F., Henderson, P. B., and Charette, M. A.:
1010 Greenland meltwater as a significant and potentially bioavailable source of iron to the ocean,
1011 Nature Geoscience, 2013, 274-278, 10.1038/ngeo1746, 2013.
1012 Bonnet, S., and Guieu, C.: Dissolution of atmospheric iron in seawater, Geophysical Research Letters,
1013 31, 10.1029/2003gl018423, 2004.
1014 Bonnet, S., and Guieu, C.: Atmospheric forcing on the annual iron cycle in the western Mediterranean
1015 Sea: A 1-year survey, Journal of Geophysical Research, 111, 10.1029/2005jc003213, 2006.
1016 Boyd, P. W., Watson, A. J., Law, C. S., Abraham, E. R., Trull, T., Murdoch, R., Bakker, D. C. E.,
1017 Bowie, A. R., Buesseler, K. O., Chang, H., Charette, M., Croot, P., Downing, K., Frew, R., Gall, M.,
1018 Hadfield, M., Hall, J., Harvey, M., Jameson, G., LaRoche, J., Liddicoat, M., Ling, R., Maldonado, M.
1019 T., McKay, R. M., Nodder, S., Pickmere, S., Pridmore, R., Rintoul, S., Safi, K., Sutton, P., Strzepek,
1020 R., Tanneberger, K., Turner, S., Waite, A., and Zeldis, J.: A mesoscale phytoplankton bloom in the
1021 polar Southern Ocean stimulated by iron fertilization, Nature, 407, 695-702, 10.1038/35037500,
1022 2000.
1023 Boyd, P. W., and Ellwood, M. J.: The biogeochemical cycle of iron in the ocean, Nature Geoscience,
1024 3, 675-682, 10.1038/ngeo964, 2010.
1025 Boyd, P. W., Ibisanmi, E., Sander, S. G., Hunter, K. A., and Jackson, G. A.: Remineralization of upper
1026 ocean particles: Implications for iron biogeochemistry, Limnology and Oceanography, 55, 1271-
1027 1288, 10.4319/lo.2010.55.3.1271, 2010.

Buck, C. S., Landing, W. M., Resing, J. A., and Measures, C. I.: The solubility and deposition of aerosol Fe and other trace elements in the North Atlantic Ocean: Observations from the A16N CLIVAR/CO2 repeat hydrography section, Marine Chemistry, 120, 57-70, 10.1016/j.marchem.2008.08.003, 2010.

Canário, J., Vale, C., Caetano, M., and Madureira, M. J.: Mercury in contaminated sediments and pore waters enriched in sulphate (Tagus Estuary, Portugal), Environmental Pollution, 126, 425-433, 10.1016/S0269-7491(03)00234-3, 2003.

Charette, M. A., Morris, P. J., Henderson, P. B., and Moore, W. S.: Radium isotope distributions during the US GEOTRACES North Atlantic cruises, Marine Chemistry, 177, 184-195, 10.1016/j.marchem.2015.01.001, 2015.

Chen, Y. J.: Influence of the Iceland mantle plume on crustal accretion at the inflated Reykjanes Ridge: Magma lens and low hydrothermal activity, Journal of Geophysical Research, 108, 2524, https://doi-org.inee.bib.cnrs.fr/10.1029/2001JB000816, 2003.

Chester, R., Murphy, K. J. T., Lin, F. J., Berry, A. S., Bradshaw, G. A., and Corcoran, P. A.: Factors controlling the solubilities of trace-metals from nonremote aerosols deposited to the sea-surface by the dry deposition mode, Marine Chemistry, 42, 107-126, 10.1016/0304-4203(93)90241-f, 1993.

Conway, T. M., and John, S. G.: Quantification of dissolved iron sources to the North Atlantic Ocean, Nature, 511, 212-215, 10.1038/nature13482, 2014.

Cooper, L. W., Whitledge, T. E., Grebmeier, J. M., and Weingartner, T.: The nutrient, salinity, and stable oxygen isotope composition of Bering and Chukchi Seas waters in and near the Bering Strait, Journal of Geophysical Research, 102, 12,563-512,573, 1997.

Cooper, L. W., McClelland, J. W., Holmes, R. M., Raymond, P. A., Gibson, J. J., Guay, C. K., and Peterson, B. J.: Flow-weighted values of runoff tracers (□18O, DOC, Ba, alkalinity) from the six largest Arctic rivers, Geophysical Research Letters, 35, 1-5, 10.1029/2008GL035007, 2008.

Crane, K., Johnson, L., Appelgate, B., Nishimura, C., Buck, R., Jones, C., Vogt, P., and Kos'yan, R. Volcanic and Seismic Swarm Events on the Reykjanes Ridge and Their Similarities to Events on Iceland: Results of a Rapid Response Mission. Marine Geophysical Researches (1997) 19: 319. https://doi.org/10.1023/A:1004298425881

1057 Croot, P. L., Streu, P. and Baker, A. R.: Short residence time for iron in surface seawater impacted by
1058 atmospheric dry deposition from Saharan dust events, Geophys. Res. Lett., 31(L23S08), doi:
1059 10.1029/2004GL020153, 2004.
1060 Cutter, G., Casciotti, K., Croot, P., Geibert, W., Heimburger, L. E., Lohan, M., Planquette, H., and van
1061 de Flierdt, T.: Sampling and the Sample-handling Protocols for GEOTRACES Cruises, 2017.
1062 Daniault, N., Mercier, H., Lherminier, P., Sarafanov, A., Falina, A., Zunino, P., Pérez, F. F., Ríos, A. F.,
1063 Ferron, B., Huck, T., Thierry, V., and Gladyshev, S.: The northern North Atlantic Ocean mean
1064 circulation in the early 21st century, Progress in Oceanography, 146, 142-158,
1065 10.1016/j.pocean.2016.06.007, 2016.
1066 de Baar, H. J. W. and de Jong, J. T. M.: Distributions, Sources and Sinks of Iron in Seawater, in
1067 Biogeochemistry of Fe in Seawater, vol. Chapter 5, edited by D. R. Turner and K. A. Hunter, pp.
1068 123–253, SCOR-IUPAC series, J Wiley, Baltimore., 2001.
1069 de Barros, M. C.: A case study of waste inputs in the Tagus estuary, in: The role of the Oceans as a
1070 Waste Disposal Option, edited by: Kullenberg, G., NATO ASI Series; Series C: Mathematical and
1071 Physical Sciences, 172, Springer Netherlands, 307-324, 1986.
1072 de Jong, M. F., van Aken, H. M., Våge, K., and Pickart, R. S.: Convective mixing in the central
1073 Irminger Sea: 2002–2010, Deep Sea Research Part I: Oceanographic Research Papers, 63, 36-
1074 51, 10.1016/j.dsr.2012.01.003, 2012.
1075 Dehairs, F., Shopova, D., Ober, S., Veth, C., and Goeyens, L.: Particulate barium stocks and oxygen
1076 consumption in the Southern Ocean mesopelagic water column during spring and early summer:
1077 Relationship with export production, Deep Sea Research II, 44, 497-516, 10.1016/S0967-
1078 0645(96)00072-0, 1997.
1079 Deng, F., Henderson, G. M., Castrillejo, M., and Perez, F. F.: Evolution of ^{231}Pa and ^{230}Th in overflow
1080 waters of the North Atlantic, Biogeosciences, 15, 7299–7313, https://doi.org/10.5194/bg-15-7299-
1081 2018, 2018.
1082 Fagel, N., Robert, C., and Hilaire-Marcel, C.: Clay mineral signature of the NW Atlantic Boundary
1083 Undercurrent, Marine Geology, 130, 19-28, https://doi.org/10.1016/0025-3227(95)00134-4, 1996.
1084 Fagel, N., Robert, C., Preda, M., and Thorez, J.: Smectite composition as a tracer of deep circulation:
1085 the case of the Northern North Atlantic, Marine Geology, 172, 309-330,
1086 https://doi.org/10.1016/S0025-3227(00)00123-7, 2001.

1087 Ferron, B., Kokoszka, F., Mercier, H., Lherminier, P., Huck, T., Rios, A., and Thierry, V.: Variability of
1088 the Turbulent Kinetic Energy Dissipation along the A25 Greenland–Portugal Transect Repeated
1089 from 2002 to 2012, Journal of Physical Oceanography, 46, 1989-2003, 10.1175/jpo-d-15-0186.1,
1090 2016.
1091 Figueres, G., Martin, J. M., Meybeck, M., and Seyler, P.: A comparative study of mercury
1092 contamination in the Tagus estuary (Portugal) and major French estuaries (Gironde, Loire, Rhone),
1093 Estuarine, Coastal and Shelf Science, 20, 183-203, https://doi.org/10.1016/0272-7714(85)90037-X,
1094 1985.
1095 Fiuza, A.: Hidrologia e dinamica das aguas costeiras de Portugal, Ph. D., Universidade de Lisboa,
1096 Lisboa, Portugal, unpublished, 1984.
1097 Follows, M., and Dutkiewicz, S.: Meteorological modulation of the North Atlantic Spring Bloom, Deep
1098 Sea Research Part II: Topical Studies in Oceanography, 49, 321-344,
1099 https://doi.org/10.1016/S0967-0645(01)00105-9, 2001.
1100 García-Ibáñez, M. I., Pardo, P. C., Carracedo, L. I., Mercier, H., Lherminier, P., Ríos, A. F., and Pérez,
1101 F. F.: Structure, transports and transformations of the water masses in the Atlantic Subpolar Gyre,
1102 Progress in Oceanography, 135, 18-36, 10.1016/j.pocean.2015.03.009, 2015.
1103 García-Ibáñez, M. I., Pérez, F. F., Lherminier, P., Zunino, P., Mercier, H., and Tréguer, P.: Water
1104 mass distributions and transports for the 2014 GEOVIDE cruise in the North Atlantic,
1105 Biogeosciences, 15, 2075-2090, 10.5194/bg-15-2075-2018, 2018.
1106 Gaudencio, M. J., Guerra, M. T., and Glemarec, M.: Recherches biosedimentaires sur la zone
1107 maritime de l'estuaire du Tage, Portugal: donnees sedimentaires preliminaires. , in: Estuaries and
1108 Coasts: Spatial and Temporal Intercomparisons, edited by: Elliot, M., and Ducrotoy, J. C., Olsen
1109 and Olsen, Fredensborg, 11-16, 1991.
1110 German, C. R., Briem, J., Chin, C. S., Danielsen, M., Holland, S., James, R. H., Jonsdottir, A.,
1111 Ludford, E., Moser, C., Olafsson, J., Palmer, M. R., and Rudnicki, M. D.: Hydrothermal activity on
1112 the Reykjanes Ridge: the Steinahóll vent-field at 63°06′N, Earth and Planetary Science Letters,
1113 121, 647-654, https://doi.org/10.1016/0012-821X(94)90098-1, 1994.
1114 Gerringa, L. J. A., Blain, S., Laan, P., Sarthou, G., Veldhuis, M. J. W., Brussaard, C. P. D., Viollier, E.,
1115 and Timmermans, K. R.: Fe-binding dissolved organic ligands near the Kerguelen Archipelago in
1116 the Southern Ocean (Indian sector), Deep Sea Research Part II: Topical Studies in Oceanography,
1117 55, 606-621, 10.1016/j.dsr2.2007.12.007, 2008.

Gerringa, L. J. A., Rijkenberg, M. J. A., Schoemann, V., Laan, P. and de Baar, H. J. W.: Organic complexation of iron in the West Atlantic Ocean, Marine Chemistry, 177, 434–446, doi:10.1016/j.marchem.2015.04.007, 2015.

Gerringa, L. J. A., Slagter, H. A., Bown, J., van Haren, H., Laan, P., de Baar, H. J. W., and Rijkenberg, M. J. A.: Dissolved Fe and Fe-binding organic ligands in the Mediterranean Sea – GEOTRACES G04, Marine Chemistry, 194, 100-113, 10.1016/j.marchem.2017.05.012, 2017.

Gourain, A., Planquette, H., Cheize, M., Lemaitre, N., Menzel Barraqueta, J.-L., Shelley, R., Lherminier, P., and Sarthou, G.: Inputs and processes affecting the distribution of particulate iron in the North Atlantic along the GEOVIDE (GEOTRACES GA01) section, Biogeosciences, 16, 1563–1582, https://doi.org/10.5194/bg-16-1563-2019, 2019.

Guerzoni, S., Chester, R., Dulac, F., Herut, B., Loye-Pilot, M.-D., Measures, C., Migon, C., Molinaroli, E., Moulin, C., Rossini, P., Saydam, C., Soudine, A., and Ziveri, P.: The role of atmospheric deposition in the biogeochemistry of the Mediterranean Sea, Progress in Oceanography, 44, 147-190, https://doi.org/10.1016/S0079-6611(99)00024-5, 1999.

Guieu, C., Loÿe-Pilot, M. D., Benyahya, L., and Dufour, A.: Spatial variability of atmospheric fluxes of metals (Al, Fe, Cd, Zn and Pb) and phosphorus over the whole Mediterranean from a one-year monitoring experiment: Biogeochemical implications, Marine Chemistry, 120, 164-178, 10.1016/j.marchem.2009.02.004, 2010.

Guieu, C., Aumont, O., Paytan, A., Bopp, L., Law, C. S., Mahowald, N., Achterberg, E. P., Marañón, E., Salihoglu, B., Crise, A., Wagener, T., Herut, B., Desboeufs, K., Kanakidou, M., Olgun, N., Peters, F., Pulido-Villena, E., Tovar-Sanchez, A., and Völker, C.: The significance of the episodic nature of atmospheric deposition to Low Nutrient Low Chlorophyll regions, Global Biogeochemical Cycles, 28, 1179-1198, 10.1002/2014gb004852, 2014.

Harrison, W. G., Yngve Børsheim, K., Li, W. K. W., Maillet, G. L., Pepin, P., Sakshaug, E., Skogen, M. D., and Yeats, P. A.: Phytoplankton production and growth regulation in the Subarctic North Atlantic: A comparative study of the Labrador Sea-Labrador/Newfoundland shelves and Barents/Norwegian/Greenland seas and shelves, Progress in Oceanography, 114, 26-45, 10.1016/j.pocean.2013.05.003, 2013.

Hatta, M., Measures, C. I., Wu, J., Roshan, S., Fitzsimmons, J. N., Sedwick, P., and Morton, P.: An overview of dissolved Fe and Mn distributions during the 2010-2011 US GEOTRACES north

Atlantic cruises: GEOTRACES GA03, Deep-Sea Research Part Ii-Topical Studies in Oceanography, 116, 117-129, 10.1016/j.dsr2.2014.07.005, 2015.

Hawkings, J. R., Wadham, J. L., Tranter, M., Raiswell, R., Benning, L. G., Statham, P. J., Tedstone, A., Nienow, P., Lee, K., and Telling, J.: Ice sheets as a significant source of highly reactive nanoparticulate iron to the oceans, Nature communications, 5, 1-8, 10.1038/ncomms4929, 2014.

Henson, S. A., Dunne, J. P., and Sarmiento, J. L.: Decadal variability in North Atlantic phytoplankton blooms, Journal of Geophysical Research, 114, 10.1029/2008jc005139, 2009.

Ho, T.-Y., Quigg, A., Finkel, Z. V., Milligan, A. J., Wyman, K., Falkowski, P. G., and Morel, F. M. M.: The elemental composition of some marine phytoplankton, Journal of Phycology, 39, 1145-1159, https://doi.org/10.1111/j.0022-3646.2003.03-090.x, 2003.

Homoky, W. B., Hembury, D. J., Hepburn, L. E., Mills, R. A., Statham, P. J., Fones, G. R., and Palmer, M. R.: Iron and manganese diagenesis in deep sea volcanogenic sediments and the origins of pore water colloids, Geochimica Et Cosmochimica Acta, 75, 5032-5048, 10.1016/j.gca.2011.06.019, 2011.

Homoky, W. B., John, S. G., Conway, T. M., and Mills, R. A.: Distinct iron isotopic signatures and supply from marine sediment dissolution, Nature Communications, 4, 10.1038/ncomms3143, 2013.

Humphreys, M. P., Griffiths, A. M., Achterberg, E. P., Holliday, N. P., Rérolle, V., Menzel Barraqueta, J. L., Couldrey, M. P., Oliver, K. I., Hartman, S. E., and Esposito, M.: Multidecadal accumulation of anthropogenic and remineralized dissolved inorganic carbon along the Extended Ellett Line in the northeast Atlantic Ocean, Global Biogeochemical Cycles, 30, 293-310, doi: 10.1002/2015GB005246, 2016.

Hunke, E. C., Notz, D., Turner, A. K., and Vancoppenolle, M.: The multiphase physics of sea ice: a review for model developers, The Cryosphere, 5, 989-1009, 10.5194/tc-5-989-2011, 2011.

Janssens, J., Meiners, K. M., Tison, J.-L., Dieckmann, G., Delille, B., and Lannuzel, D.: Incorporation of iron and organic matter into young Antarctic sea ice during its initial growth stages, Elementa: Science of the Anthropocene, 4, 000123, 10.12952/journal.elementa.000123, 2016.

Jickells, T., and Moore, C. M.: The importance of atmospheric deposition for ocean productivity, Annual Review of Ecology, Evolution, and Systematics, 46, 481-501, 10.1146/annurev-ecolsys-112414-054118, 2015.

Jickells, T. D., An, Z. C., Andersen, K. K., Baker, A. R., Bergametti, G., Brooks, N., Cao, J. J., Boyd, P. W., Duce, R. A., Hunter, K. A., Kawahata, H., Kubilay, N., laRoche, J., Liss, P. S., Mahowald, N.,

Prospero, J. M., Ridgwell, A. J., Tegen, I., and Torres, R.: Global iron connections between desert dust, ocean biogeochemistry, and climate, Science, 308, 67-71, DOI: 10.1126/science.1105959, 2005.

Jones, E. P., Anderson, L. G., and Swift, J. H.: Distribution of Atlantic and Pacific waters in the upper Arctic Ocean: Implications for circulation, Geophysical Research Letters, 25, 765-768, https://doi-org.inee.bib.cnrs.fr/10.1029/98GL00464, 1998.

Kan, C. C., Chen, W. H., Wan, M. W., Phatai, P., Wittayakun, J., and Li, K. F.: The preliminary study of iron and manganese removal from groundwater by NaOCl oxidation and MF filtration, Sustain. Environ. Res., 22, 25-30, 2012.

Kanzow, T. and Zenk, W.: Structure and transport of the Iceland Scotland Overflow plume along the Reykjanes Ridge in the Iceland Basin, Deep Sea Research Part I: Oceanographic Research Papers, 86, 82–93, doi:10.1016/j.dsr.2013.11.003, 2014

Kara, A. B., Rochford, P. A., and Hurlburt, H. E.: An optimal definition for ocean mixed layer depth, Journal of Geophysical Research, 105, 16,803-816,821, 10.1029/2000JC900072, 2000.

Käse, R. H., Girton, J. B. and Sanford, T. B.: Structure and variability of the Denmark Strait Overflow: Model and observations, Journal of Geophysical Research: Oceans, 108(C6), doi:10.1029/2002JC001548, 2003.

Kissel, C., Laj, C., Mulder, T., Wandres, C., and Cremer, M.: The magnetic fraction: A tracer of deep water circulation in the North Atlantic, Earth and Planetary Science Letters, 288, 444-454, 10.1016/j.epsl.2009.10.005, 2009.

Klunder, M. B., Bauch, D., Laan, P., de Baar, H. J. W., van Heuven, S. M. A. C., and Ober, S.: Dissolved iron in the Arctic shelf seas and surface waters of the Central Arctic Ocean: impact of Arctic river water and ice-melt, Journal of Geophysical Research, 117, 1-18, https://doi-org.inee.bib.cnrs.fr/10.1029/2011JC007133, 2012.

Lackschewitz, K. S., Endler, R., Gehrke, B., Wallrabe-Adams, H.-J., and Thiede, J.: Evidence for topography- and current-controlled deposition on the reykjanes Ridge between 59°N and 60°N, Deep-Sea Research I, 43, 1683-1711, https://doi.org/10.1016/S0967-0637(96)00090-8, 1996.

Laes, A., Blain, S., Laan, P., Achterberg, E. P., Sarthou, G., and de Baar, H. J. W.: Deep dissolved iron profiles in the eastern North Atlantic in relation to water masses, Geophysical Research Letters, 30, 10.1029/2003gl017902, 2003.

Lagerström, M. E., Field, M. P., Seguret, M., Fischer, L., Hann, S., and Sherrell, R. M.: Automated on-line flow-injection ICP-MS determination of trace metals (Mn, Fe, Co, Ni, Cu and Zn) in open ocean seawater: Application to the GEOTRACES program, Marine Chemistry, 155, 71-80, 10.1016/j.marchem.2013.06.001, 2013.

Lambelet, M., van de Flierdt, T., Crocket, K., Rehkamper, M., Katharina, K., Coles, B., Rijkenberg, M. J. A., Gerringa, L. J. A., de Baar, H. J. W., and Steinfeldt, R.: Neodymium isotopic composition and concentration in the western North Atlantic Ocean: Results from the GEOTRACES GA02 section, Geochimica Et Cosmochimica Acta, 177, 1-29, https://doi.org/10.1016/j.gca.2015.12.019, 2016.

Le Roy, E., Sanial, V., Charette, M. A., van Beek, P., Lacan, F., Jacquet, S. H. M., Henderson, P. B., Souhaut, M., García-Ibáñez, M. I., Jeandel, C., Pérez, F. F., and Sarthou, G.: The ^{226}Ra–Ba relationship in the North Atlantic during GEOTRACES-GA01, Biogeosciences, 15, 3027-3048, 10.5194/bg-15-3027-2018, 2018.

Lemaitre, N., Planchon, F., Planquette, H., Dehairs, F., Fonseca-Batista, D., Roukaerts, A., Deman, F., Tang, Y., Mariez, C., and Sarthou, G.: High variability of particulate organic carbon export along the North Atlantic GEOTRACES section GA01 as deduced from 234Th fluxes, Biogeosciences, 15, 6417–6437, https://doi.org/10.5194/bg-15-6417-2018, 2018. .

Lemaitre, N., Planquette, H., Planchon, F., Sarthou, G., Jacquet, S., García-Ibáñez, M. I., Gourain, A., Cheize, M., Monin, L., André, L., Laha, P., Terryn, H., and Dehairs, F.: Particulate barium tracing of significant mesopelagic carbon remineralisation in the North Atlantic, Biogeosciences, 15, 2289–2307, https://doi.org/10.5194/bg-15-2289-2018, 2018.

Lohan, M. C., and Bruland, K. W.: Elevated Fe(II) and Dissolved Fe in Hypoxic Shelf Waters off Oregon and Washington: An Enhanced Source of Iron to Coastal Upwelling Regimes, Environmental Science & Technology, 42, 6462-6468, 10.1021/es800144j, 2008.

Longhurst, A. R.: Ecological geography of the Sea, Second Edition ed., Elsevier Academic Press publications, Burlington, 542 pp., 2007.

Louanchi, F., and Najjar, R. G.: Annual cycles of nutrients and oxygen in the upper layers of the North Atlantic Ocean, Deep Sea Research Part II: Topical Studies in Oceanography, 48, 2155-2171, https://doi.org/10.1016/S0967-0645(00)00185-5, 2001.

Markus, T., Stroeve, J. C., and Miller, J.: Recent changes in Arctic sea ice melt onset, freezeup, and melt season length, Journal of Geophysical Research, 114, 10.1029/2009jc005436, 2009.

1239 Marshall, J., and Schott, F.: Open-ocean convection: observations, theory, and models, Reviews of
1240 Geophysics, 37, 1-64, doi: 10.1029/98RG02739, 1999.
1241 Martin, J.-M., Elbaz-Poulichet, F., Guieu, C., Loÿe-Pilot, M.-D., and Han, G.: River versus atmospheric
1242 input of material to the Mediterranean Sea: an overview, Marine Chemistry, 28, 159-182,
1243 https://doi.org/10.1016/0304-4203(89)90193-X, 1989.
1244 Martin, J. D., and Fitzwater, S. E.: Iron deficiency limits phytoplankton growth in the north-east Pacific
1245 subarctic, Nature, 331, 341-343, 1988.
1246 Martin, J. H., Fitzwater, S. E., and Gordon, R. M.: Iron deficiencies limits phytoplankton growth in
1247 Antarctic waters, Global Biogeochemical Cycles, 4, 5-12, https://doi-
1248 org.inee.bib.cnrs.fr/10.1029/GB004i001p00005, 1990.
1249 Martin, J. H., Coale, K. H., Johnson, K. S., Fitzwater, S. E., Gordon, R. M., Tanner, S. J., Hunter, C.
1250 N., Elrod, V. A., Nowicki, J. L., Coley, T. L., Barber, R. T., Lindley, S., Watson, A. J., Van Scoy, K.,
1251 Law, C. S., Liddicoat, M. I., Ling, R., Stanton, T., Stockel, J., Collins, C., Anderson, A., Bidigare, R.,
1252 Ondrusek, M., Latasa, M., Millero, F. J., Lee, K., Yao, W., Zhang, J. Z., Friederich, G., Sakamoto,
1253 C., Chavez, F., Buck, K., Kolber, Z., Greene, R., Falkowski, P., Chisholm, S. W., Hoge, F., Swift,
1254 R., Yungel, J., Turner, S., Nightingale, P., Hatton, A., Liss, P., and Tindale, N. W.: Testing the Iron
1255 Hypothesis in Ecosystems of the Equatorial Pacific Ocean, Nature, 371, 123-129,
1256 10.1038/371123a0, 1994.
1257 Measures, C. I., Brown, M. T., Selph, K. E., Apprill, A., Zhou, M., Hatta, M., and Hiscock, W. T.: The
1258 influence of shelf processes in delivering dissolved iron to the HNLC waters of the Drake Passage,
1259 Antarctica, Deep Sea Research Part II: Topical Studies in Oceanography, 90, 77-88,
1260 10.1016/j.dsr2.2012.11.004, 2013.
1261 Melling, H., and Moore, R. M.: Modification of halocline source waters during freezing on the Beaufort
1262 Sea shelf: Evidence from oxygen isotopes and dissolved nutrients, Continental Shelf Research, 15,
1263 89-113, https://doi.org/10.1016/0278-4343(94)P1814-R, 1995.
1264 Menzel Barraqueta, J.-L., Schlosser, C., Planquette, H., Gourain, A., Cheize, M., Boutorh, J., Shelley,
1265 R., Contreira Pereira, L., Gledhill, M., Hopwood, M. J., Lacan, F., Lherminier, P., Sarthou, G., and
1266 Achterberg, E. P.: Aluminium in the North Atlantic Ocean and the Labrador Sea (GEOTRACES
1267 GA01 section): roles of continental inputs and biogenic particle removal, Biogeosciences, 15,
1268 5271–5286, https://doi.org/10.5194/bg-15-5271-2018, 2018. .

Mercier, H., Lherminier, P., Sarafanov, A., Gaillard, F., Daniault, N., Desbruyères, D., Falina, A., Ferron, B., Gourcuff, C., Huck, T., and Thierry, V.: Variability of the meridional overturning circulation at the Greenland–Portugal OVIDE section from 1993 to 2010, Progress in Oceanography, 132, 250-261, 10.1016/j.pocean.2013.11.001, 2015.

Mil-Homens, M., Branco, V., Lopes, C., Vale, C., Abrantes, F., Boer, W., and Vicente, M.: Using factor analysis to charactierise historical trends of trace metal contamination in a sediment core from the Tagus Prodelta, Portugal, Water, Air, and Soil Pollution, 197, 277-287, https://doi.org/10.1007/s11270-008-9810-0, 2009.

Moore, C. M., Mills, M. M., Langlois, R., Milne, A., Achterberg, E. P., La Roche, J., and Geider, R. J.: Relative influence of nitrogen and phosphorus availability on phytoplankton physiology and productivity in the oligotrophic sub-tropical North Atlantic Ocean, Limnology and Oceanography, 53, 291-205, https://doi-org.inee.bib.cnrs.fr/10.4319/lo.2008.53.1.0291, 2008.

Moore, C. M., Mills, M. M., Arrigo, K. R., Berman-Frank, I., Bopp, L., Boyd, P. W., Galbraith, E. D., Geider, R. J., Guieu, C., Jaccard, S. L., Jickells, T. D., La Roche, J., Lenton, T. M., Mahowald, N. M., Marañón, E., Marinov, I., Moore, J. K., Nakatsuka, T., Oschlies, A., Saito, M. A., Thingstad, T. F., Tsuda, A., and Ulloa, O.: Processes and patterns of oceanic nutrient limitation, Nature Geoscience, 6, 701-710, 10.1038/ngeo1765, 2013.

Moore, G. W. K.: Gale force winds over the Irminger Sea to the east of Cape Farewell, Greenland, Geophysical Research Letters, 30, 17, 10.1029/2003gl018012, 2003.

Nielsdóttir, M. C., Moore, C. M., Sanders, R., Hinz, D. J., and Achterberg, E. P.: Iron limitation of the postbloom phytoplankton communities in the Iceland Basin, Global Biogeochemical Cycles, GB3001, doi:10.1029/2008GB003410, 2009.

Olaffson, J., Thors, K., and Cann, J. R.: A sudden cruise off Iceland, RIDGE Events, 2, 35-28, 1991.

Oschlies, A.: Nutrient supply to the surface waters of the North Atlantic: A model study, Journal of Geophysical Research, 107, 10.1029/2000jc000275, 2002.

Painter, S. C., Henson, S. A., Forryan, A., Steigenberger, S., Klar, J., Stinchcombe, M. C., Rogan, N., Baker, A. R., Achterberg, E. P., and Moore, C. M.: An assessment of the vertical diffusive flux of iron and other nutrients to the surface waters of the subpolar North Atlantic Ocean, Biogeosciences, 11, 2113-2130, 10.5194/bg-11-2113-2014, 2014.

Palmer, M. R., Ludford, E. M., German, C. R., and Lilley, M. D.: Dissolved methane and hydrogen in the Steinahóll hydrothermal plume, 63°N, Reykjanes Ridge, in: Hydrothermal Vents and

Processes, edited by: Parson, L. M., Walker, C. L., and Dixon, D. R., Special Publications, Geological Society, London, 111-120, 1995.
Parekh, P., Follows, M. J., and Boyle, E. A.: Decoupling of iron and phosphate in the global ocean, Global Biogeochemical Cycle, 19, GB2020, https://doi-org.inee.bib.cnrs.fr/10.1029/2004GB002280, 2005.
Parra, M., Delmont, P., Ferragne, A., Latouche, C., Pons, J. C., and Puechmaille, C.: Origin and evolution of smectites in recent marine sediments of the NE Atlantic, Clay Minerals, 20, 335-346, https://doi.org/10.1180/claymin.1985.020.3.06, 1985.
Pérez, F. F., Mercier, H., Vázquez-Rodríguez, M., Lherminier, P., Velo, A., Pardo, P. C., Rosón, G., and Ríos, A. F.: Atlantic Ocean CO2 uptake reduced by weakening of the meridional overturning circulation, Nature Geoscience, 6, 146-152, 10.1038/ngeo1680, 2013.
Pérez, F. F., Treguer, P., Branellec, P., García-Ibáñez, M. I., Lherminier, P., and Sarthou, G.: The 2014 Greenland-Portugal GEOVIDE bottle data (GO-SHIP A25 and GEOTRACES GA01). SEANOE (Ed.), 2018.
Petrich, C., and Eicken, H.: Growth, structure and properties of sea ice, in: Sea Ice. 2nd ed., edited by: Thomas, D. N., and Dieckmann, G. S., Wiley-Blackwell, Oxford, U.K., 23-77, 2010.
Pickart, R. S., Straneo, F., and Moore, G. W. K.: Is Labrador Sea Water formed in the Irminger basin?, Deep Sea Research Part I:, 50, 23-52, https://doi.org/10.1016/S0967-0637(02)00134-6, 2003.
Piron, A., Thierry, V., Mercier, H., and Caniaux, G.: Argo float observations of basin-scale deep convection in the Irminger sea during winter 2011–2012, Deep Sea Research Part I: Oceanographic Research Papers, 109, 76-90, 10.1016/j.dsr.2015.12.012, 2016.
Radic, A., Lacan, F., and Murray, J. W.: Iron isotopes in the seawater of the equatorial Pacific Ocean: New constraints for the oceanic iron cycle, Earth and Planetary Science Letters, 306, 1-10, 10.1016/j.epsl.2011.03.015, 2011.
Ras, J., Claustre, H., and Uitz, J.: Spatial variability of phytoplankton pigment distribution in the Subtropical South Pacific Ocean: comparison between *in situ* and predicted data, Biogeosciences, 5, 353-369, https://doi.org/10.5194/bg-5-353-2008, 2008.
Riebesell, U., Schloss, I., and Smetacek, V.: Aggregation of algae released from melting sea ice: implications for seeding and sedimentation, Polar Biology, 11, 239-248, https://doi.org/10.1007/BF00238457, 1991.

Rijkenberg, M. J., Middag, R., Laan, P., Gerringa, L. J., van Aken, H. M., Schoemann, V., de Jong, J. T., and de Baar, H. J.: The distribution of dissolved iron in the West Atlantic Ocean, PLoS One, 9, e101323, 10.1371/journal.pone.0101323, 2014.

Sabine, C. L., Feely, R. A., Gruber, N., Key, R. M., Lee, K., Bullister, J. L., Wanninkhof, R., Wong, C. S., Wallace, D. W. R., Tilbrook, B., Millero, F. J., Peng, T.-H., Kozyr, A., Ono, T., and Rios, A. F.: The Oceanic sink for anthropogenic CO2, Science, 305, 367-371, 10.1126/science.1097403, 2004.

Sanders, R., Brown, L., Henson, S., and Lucas, M.: New production in the Irminger Basin during 2002, Journal of Marine Systems, 55, 291-310, http:// dx.doi.org/10.1016/j.jmarsys.2004.09.002, 2005.

Santos-Echeandia, J., Vale, C., Caetano, M., Pereira, P., and Prego, R.: Effect of tidal flooding on metal distribution in pore waters of marsh sediments and its transport to water column (Tagus estuary, Portugal), Mar Environ Res, 70, 358-367, 10.1016/j.marenvres.2010.07.003, 2010.

Sarthou, G., and Jeandel, C.: Seasonal variations of iron concentrations in the Ligurian Sea and iron budget in the Western Mediterranean Sea, Marine Chemistry, 74, 115-129, 10.1016/s0304-4203(00)00119-5, 2001.

Sarthou, G., Baker, A. R., Kramer, J., Laan, P., Laës, A., Ussher, S., Achterberg, E. P., de Baar, H. J. W., Timmermans, K. R., and Blain, S.: Influence of atmospheric inputs on the iron distribution in the subtropical North-East Atlantic Ocean, Marine Chemistry, 104, 186-202, 10.1016/j.marchem.2006.11.004, 2007.

Sarthou, G., Laan, P., Ussher, S., Kramer, J., Timmermans, K. R. and Blain, S.: Influence of high atmospheric inputs on the iron distribution in the water column of the North Atlantic Ocean., 2003.

Sarthou, G., Lherminier, P., Achterberg, E. P., Alonso-Pérez, F., Bucciarelli, E., Boutorh, J., Bouvier, V., Boyle, E. A., Branellec, P., Carracedo, L. I., Casacuberta, N., Castrillejo, M., Cheize, M., Contreira Pereira, L., Cossa, D., Daniault, N., De Saint-Léger, E., Dehairs, F., Deng, F., Desprez de Gésincourt, F., Devesa, J., Foliot, L., Fonseca-Batista, D., Gallinari, M., García-Ibáñez, M. I., Gourain, A., Grossteffan, E., Hamon, M., Heimbürger, L. E., Henderson, G. M., Jeandel, C., Kermabon, C., Lacan, F., Le Bot, P., Le Goff, M., Le Roy, E., Lefèbvre, A., Leizour, S., Lemaitre, N., Masqué, P., Ménage, O., Menzel Barraqueta, J.-L., Mercier, H., Perault, F., Pérez, F. F., Planquette, H. F., Planchon, F., Roukaerts, A., Sanial, V., Sauzède, R., Schmechtig, C., Shelley, R. U., Stewart, G., Sutton, J. N., Tang, Y., Tisnérat-Laborde, N., Tonnard, M., Tréguer, P., van Beek, P., Zurbrick, C. M., and Zunino, P.: Introduction to the French GEOTRACES North Atlantic

Transect (GA01): GEOVIDE cruise, Biogeosciences, 15, 7097–7109, https://doi.org/10.5194/bg-15-7097-2018, 2018.

Sarthou, G., Vincent, D., Christaki, U., Obernosterer, I., Timmermans, K. R., and Brussaard, C. P. D.: The fate of biogenic iron during a phytoplankton bloom induced by natural fertilisation: Impact of copepod grazing, Deep Sea Research Part II: Topical Studies in Oceanography, 55, 734-751, 10.1016/j.dsr2.2007.12.033, 2008.

Ocean Data View, https://odv.awi.de ODV4, version 4.7.6 (23 March 2016), access: 6 April, 2016.

Schmidt, S. and Reyss, J.-L.: Radium as internal tracer of Mediterranean Outflow Water, Journal of Geophysical Research, 101, 3589–3596, 1996.

Schroth, A. W., Crusius, J., Hoyer, I., and Campbell, R.: Estuarine removal of glacial iron and implications for iron fluxes to the ocean, Geophysical Research Letters, 41, 3951-3958, 10.1002/2014GL060199, 2014.

Shelley, R. U., Morton, P. L., and Landing, W. M.: Elemental ratios and enrichment factors in aerosols from the US-GEOTRACES North Atlantic transects, Deep Sea Research, 116, 262-272, https://doi.org/10.1016/j.dsr2.2014.12.005, 2015.

Shelley, R. U., Roca-Martí, M., Castrillejo, M., Sanial, V., Masqué, P., Landing, W. M., van Beek, P., Planquette, H., and Sarthou, G.: Quantification of trace element atmospheric deposition fluxes to the Atlantic Ocean (>40°N; GEOVIDE, GEOTRACES GA01) during spring 2014, Deep Sea Research Part I: Oceanographic Research Papers, 119, 34-49, 10.1016/j.dsr.2016.11.010, 2017.

Shelley, R. U., Landing, W. M., Ussher, S. J., Planquette, H., and Sarthou, G.: Regional trends in the fractional solubility of Fe and other metals from North Atlantic aerosols (GEOTRACES cruises GA01 and GA03) following a two-stage leach, Biogeosciences, 15, 2271–2288, https://doi.org/10.5194/bg-15-2271-2018, 2018.

Shor, A., Lonsdale, P., Hollister, D., and Spencer, D.: Charlie-Gibbs fracture zone: bottom-water transport and its geological effects, Deep Sea Research, 27A, 325-345, https://doi.org/10.1016/0198-0149(80)90030-8, 1980.

Sinha, M. C., Navin, D. A., MacGregor, L. M., Constable, S., Peirce, C., White, A., Heinson, G., and Inglis, M. A.: Evidence for accumulated melt beneath the slow-spreading Mid-Atlantic Ridge, Philosophical Transactions of the Royal Society A, 355, 233-253, https://doi.org/10.1098/rsta.1997.0008, 1997.

Slagter, H. A., Reader, H. E., Rijkenberg, M. J. A., Rutgers van der Loeff, M., de Baar, H. J. W., and Gerringa, L. J. A.: Organic Fe speciation in the Eurasian Basins of the Arctic Ocean and its relation to terrestrial DOM, Marine Chemistry, 197, 11-25, 10.1016/j.marchem.2017.10.005, 2017.

Smallwood, J. R., and White, R. S.: Crustal accretion at the Reykjanes Ridge, 61°-62°N, Journal of Geophysical Research: Solid Earth, 103, 5185-5201, 10.1029/97jb03387, 1998.

Statham, P. J., Skidmore, M., and Tranter, M.: Inputs of glacially derived dissolved and colloidal iron to the coastal ocean and implications for primary productivity, Global Biogeochemical Cycles, 22, 1-11, 10.1029/2007GB003106, 2008.

Sunda, W. G., and Huntsman, S. A.: Iron uptake and growth limitation in oceanic and coastal phytoplankton, Marine Chemistry, 50, 189-206, 10.1016/0304-4203(95)00035-p, 1995.

Sutherland, D. A., Pickart, R. S., Peter Jones, E., Azetsu-Scott, K., Jane Eert, A., and Ólafsson, J.: Freshwater composition of the waters off southeast Greenland and their link to the Arctic Ocean, Journal of Geophysical Research, 114, 10.1029/2008jc004808, 2009.

Tagliabue, A., Aumont, O., DeAth, R., Dunne, J. P., Dutkiewicz, S., Galbraith, E., Misumi, K., Moore, J. K., Ridgwell, A., Sherman, E., Stock, C., Vichi, M., Völker, C. and Yool, A.: How well do global ocean biogeochemistry models simulate dissolved iron distributions?, Global Biogeochemical Cycles, 30(2), 149–174, doi:10.1002/2015GB005289, 2016.

Tanhua, T., Olsson, K. A., and Jeansson, E.: Formation of Denmark Strait overflow water and its hydro-chemical composition, Journal of Marine Systems, 57, 264-288, 10.1016/j.jmarsys.2005.05.003, 2005.

Teng, Z., Huang, J. Y., Fujito, K., and Takizawa, S.: Manganese removal by hollow fiber micro-filter.Membrane separation for drinking water, Euroopean Conference on Desalination and the Environment, Amsterdam, 28 May, 2001.

Thuróczy, C. E., Gerringa, L. J. A., Klunder, M. B., Middag, R., Laan, P., Timmermans, K. R., and de Baar, H. J. W.: Speciation of Fe in the Eastern North Atlantic Ocean, Deep Sea Research Part I: Oceanographic Research Papers, 57, 1444-1453, 10.1016/j.dsr.2010.08.004, 2010.

Tonnard, M., Donval, A., Lampert, L., Tréguer, P., Bowie, A. R., van der Merwe, P., planquette, H., Claustre, H., Dimier, C., Ras, J., and Sarthou, G.: Phytoplankton assemblages in the North Atlantic Ocean and in the Labrador Sea along the GEOVIDE section (GEOTRACES section GA01) determined by CHEMTAX analysis from HPLC pigment data, Biogeosciences, in prep.

Tovar-Sanchez, A., Duarte, C. M., Alonso, J. C., Lacorte, S., Tauler, R., and Galban-Malagon, C.: Impacts of metals and nutrients released from melting multiyear Arctic sea ice, Journal of Geophysical Research-Oceans, 115, 10.1029/2009jc005685, 2010.

Tréguer, P. J., and De La Rocha, C. L.: The world ocean silica cycle, Ann Rev Mar Sci, 5, 477-501, 10.1146/annurev-marine-121211-172346, 2013.

Twining, B. S., Baines, S. B., Fisher, N. S., and Landry, M. R.: Cellular iron contents of plankton during the Southern Ocean Iron Experiment (SOFeX), Deep Sea Research Part I: Oceanographic Research Papers, 51, 1827-1850, 10.1016/j.dsr.2004.08.007, 2004.

Van Beusekom, J. E. E.: Distribution of aluminium in surface waters of the North Sea: influence of suspended matter., in: Biogeochemistry and Distribution of Suspended Matter in the North Sea and Implications to fisheries Biology, edited by: Kempe, S., Mittleitungen aus dem Geologisch-Paläontologischen Institut der Universität Hamburg, SCOPE/UNEP Sonderband, 117-136, 1988.

von Appen, W.-J., Koszalka, I. M., Pickart, R. S., Haine, T. W. N., Mastropole, D., Magaldi, M. G., Valdimarsson, H., Girton, J., Jochumsen, K., and Krahmann, G.: The East Greenland Spill Jet as an important component of the Atlantic Meridional Overturning Circulation, Deep Sea Research Part I: Oceanographic Research Papers, 92, 75-84, 10.1016/j.dsr.2014.06.002, 2014.

Wadhams, P.: Ice in the Ocean, Gordon and Breach Science Publishers, London, UK, 2000.

Wagener, T., Guieu, C., and Leblond, N.: Effects of dust deposition on iron cycle in the surface Mediterranean Sea: results from a mesocosm seeding experiment, Biogeosciences, 7, 3769–3781, https://doi.org/10.5194/bg-7-3769-2010, 2010. .

Woodgate, R. A., and Aagaard, K.: Revising the Bering Strait freshwater flux into the Arctic Ocean, Geophysical Research Letters, 32, 10.1029/2004GL021747., 2005.

Wuttig, K., Wagener, T., Bressac, M., Dammshäuser, A., Streu, P., Guieu, C., and Croot, P. L.: Impacts of dust deposition on dissolved trace metal concentrations (Mn, Al and Fe) during a mesocosm experiment, Biogeosciences, 10, 2583-2600, 10.5194/bg-10-2583-2013, 2013.

Yashayaev, I., Bersch, M. and Aken, H. M. van: Spreading of the Labrador Sea Water to the Irminger and Iceland basins, Geophysical Research Letters, 34(10), doi:10.1029/2006GL028999, 2007.

Zou, S., Lozier, S., Zenk, W., Bower, A., and Johns, W.: Observed and modeled pathways of the Iceland Scotland Overflow Water in the eastern North Atlantic, Progress in Oceanography, 159, 211-222, 10.1016/j.pocean.2017.10.003, 2017.

Zunino, P., Lherminier, P., Mercier, H., Daniault, N., García-Ibáñez, M. I., and Pérez, F. F.: The GEOVIDE cruise in May–June 2014 reveals an intense Meridional Overturning Circulation over a cold and fresh subpolar North Atlantic, Biogeosciences, 14, 5323–5342, https://doi.org/10.5194/bg-14-5323-2017, 2017.

Figure 1: Map of the GEOTRACES GA01 voyage plotted on bathymetry as well as the major topographical features and main basins. Crossover station with GEOTRACES voyage (GA03) is shown as a red star. (Ocean Data View (ODV) software, version 4.7.6, R. Schlitzer, http://odv.awi.de, 2016). BFZ: Bight Fracture Zone, CGFZ: Charlie-Gibbs Fracture Zone.

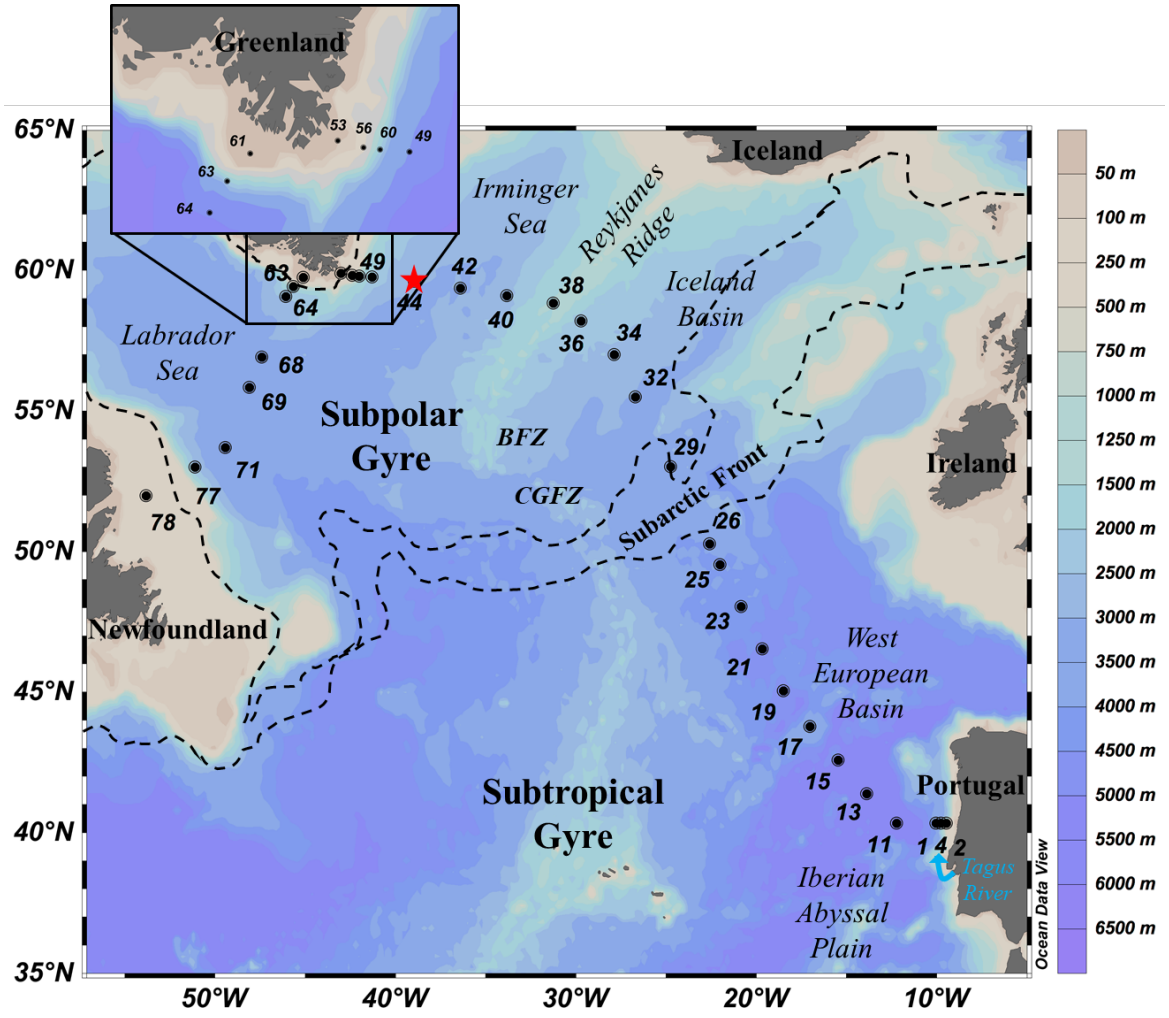

Figure 2: Parameters measured from the regular CTD cast represented as a function of depth for GA01 section for (A) Dissolved Oxygen (O_2, μmol kg^{-1}), (B) Salinity and (C) Temperature (°C). The contour lines represent isopycnals (neutral density, γ^n, in units of kg m^{-3}).

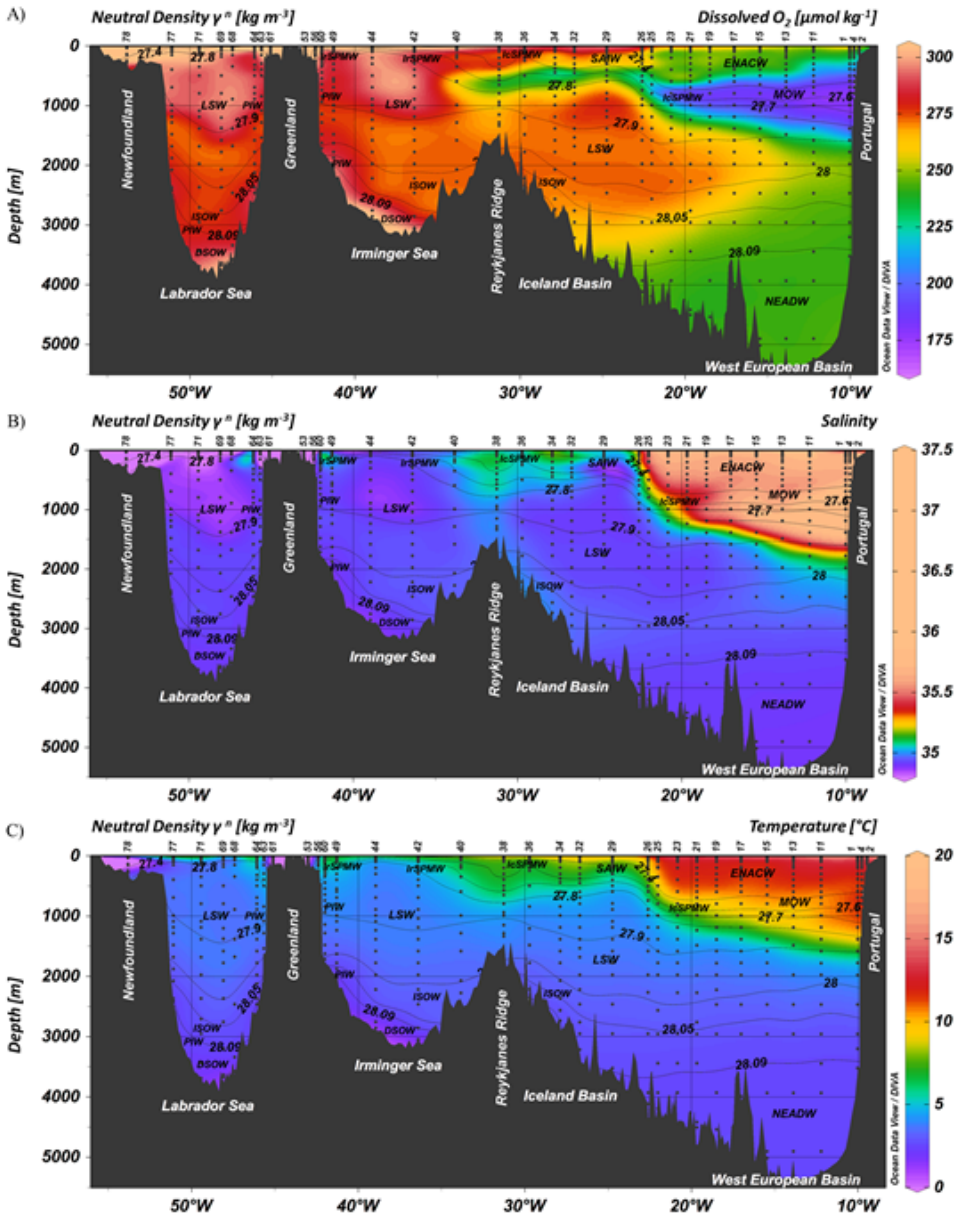

Surface water masses

ENACW	East North Atlantic Central Water
IcSPMW	Iceland SubPolar Mode Water
IrSPMW	Irminger SubPolar Mode Water
SAIW	Subarctic Intermediate Water

Intermediate water masses

MOW	Mediterranean Outflow Water
LSW	Labrador Sea Water

Overflow Deep water masses

NEADW	North East Atlantic Deep Water
PIW	Polar Intermediate Water
ISOW	Iceland-Scotland Overflow Water
DSOW	Denmark Strait Overflow Water

Figure 3: Contour plot of the distribution of dissolved iron (DFe) concentrations in nmol L^{-1} along the GA01 voyage transect: upper 1000 m (top) and full depth range (bottom). The red dashed line indicates the depth of the Surface Mixed Layer (SML). Small black dots represent collected water samples at each sampling station. (Ocean Data View (ODV) software, version 4.7.6, R. Schlitzer, http://odv.awi.de, 2016).

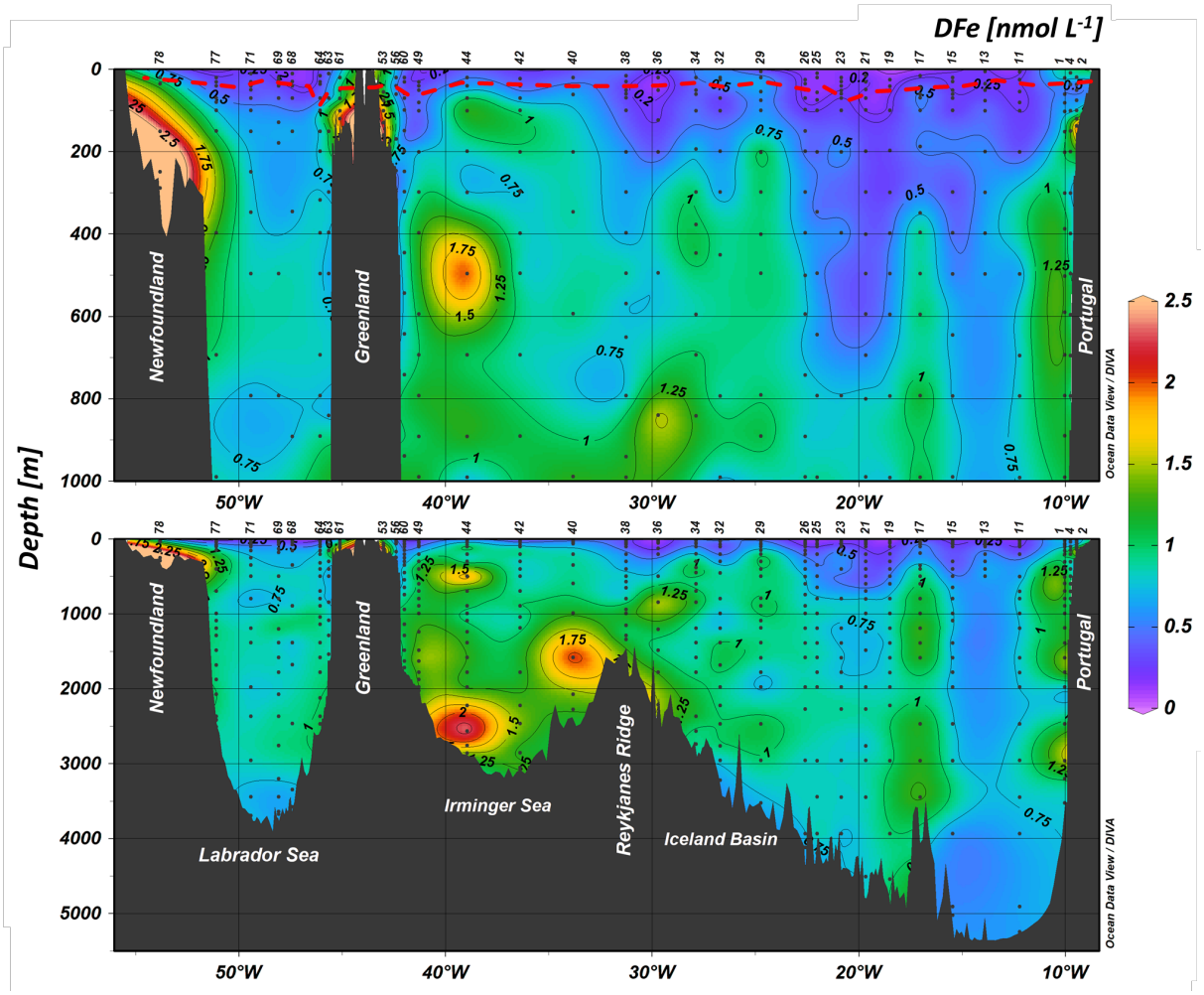

Figure 4: Vertical profiles of dissolved iron (DFe, black dots, solid line), particulate iron (PFe, black open dots, dashed line, Gourain et al., 2019) and dissolved aluminium (DAl, grey dots, Menzel Barraqueta et al., 2018) at Stations 2 (A), and 4 (B) located above the Iberian shelf, Station 56 (C), Stations 53 (D) 53 and Station 61 (E) located above the Greenland shelf and Station 78 (F) located above the Newfoundland shelf. Note that for stations 53, 61 and 78, plots of the percentage of meteoric water (open dots) and sea-ice melting (black dots and dashed line) (Benetti et al., see text for details), Total Chlorophyll-*a* (TChl-*a*, green), temperature (blue) and salinity (black) are also displayed as a function of depth.

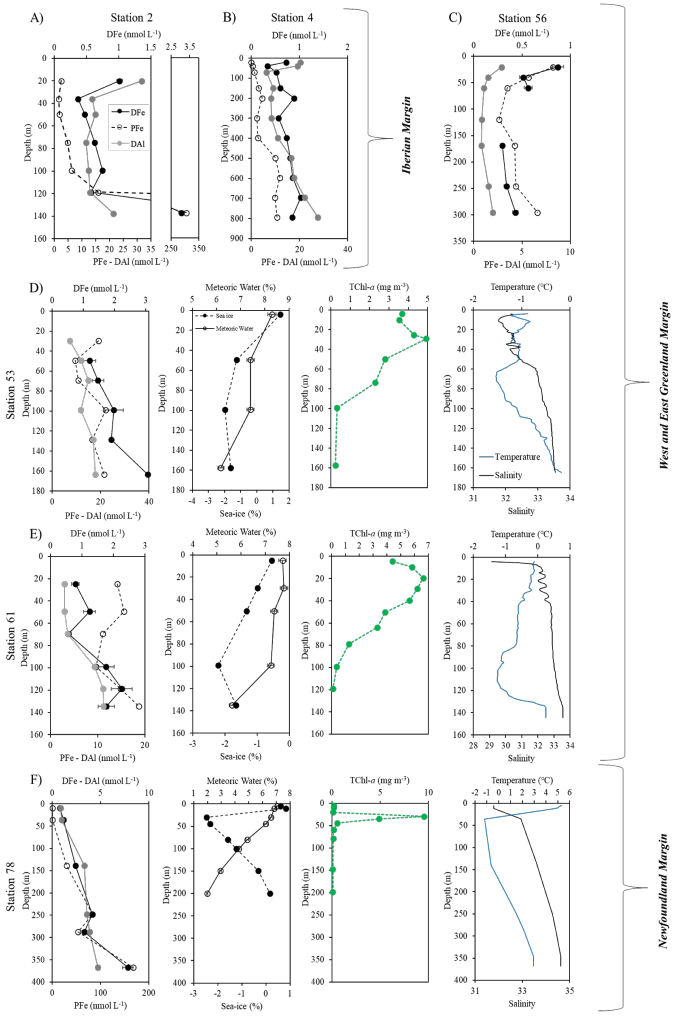

1490

Figure 5: Plot of dissolved iron (DFe, black circles) and dissolved aluminium (DAl, white circles, Menzel Barraqueta et al., 2018) at ~ 20 m, along the salinity gradient between stations 1, 2, 4, and 11 with linear regression equations. Numbers close to sample points representing station numbers.

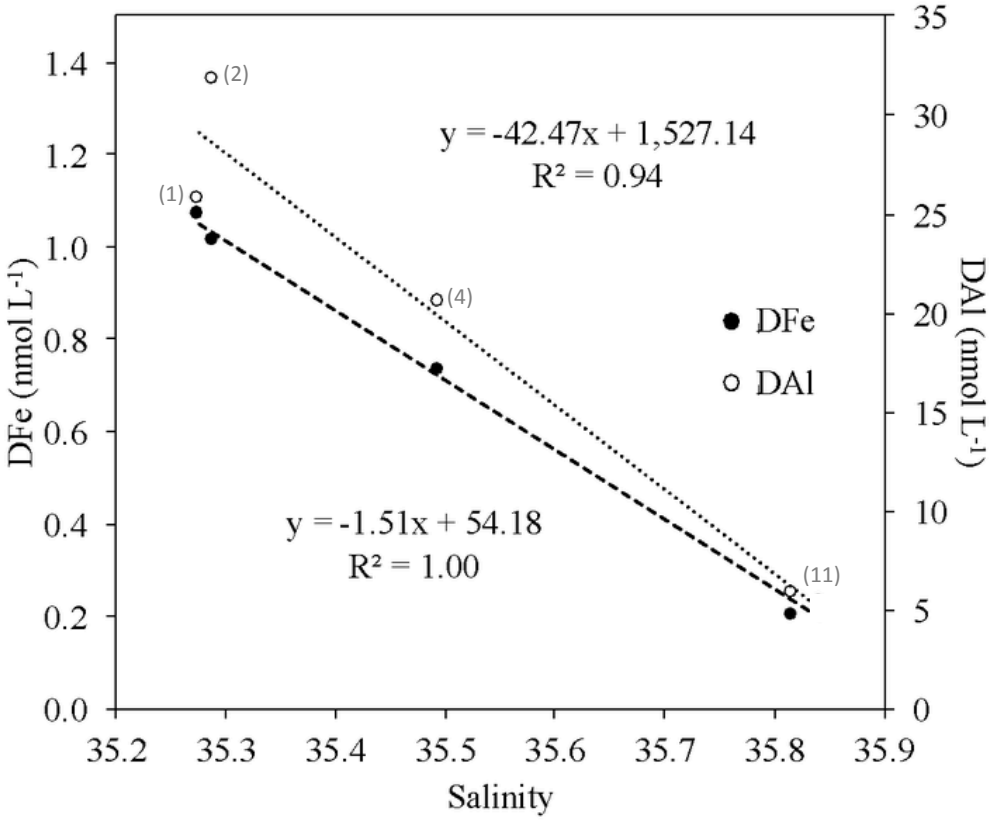

Figure 6: Plot of dissolved Fe (DFe) Turnover Times relative to Atmospheric Deposition (TTADs) calculated from soluble Fe contained in aerosols estimated from a two-stage sequential leach (UHP water, then 25% HAc, Shelley et al., this issue). Note that numbers on top of points represent station numbers and that the colour coding refers to different region with in yellow, margin stations; in purple, the West European Basin; in blue, the Iceland Basin; in green, the Irminger Sea and in red, the Labrador Sea. The numbers on top of the plot represent TTADs averaged for each oceanic basin and their standard deviation.

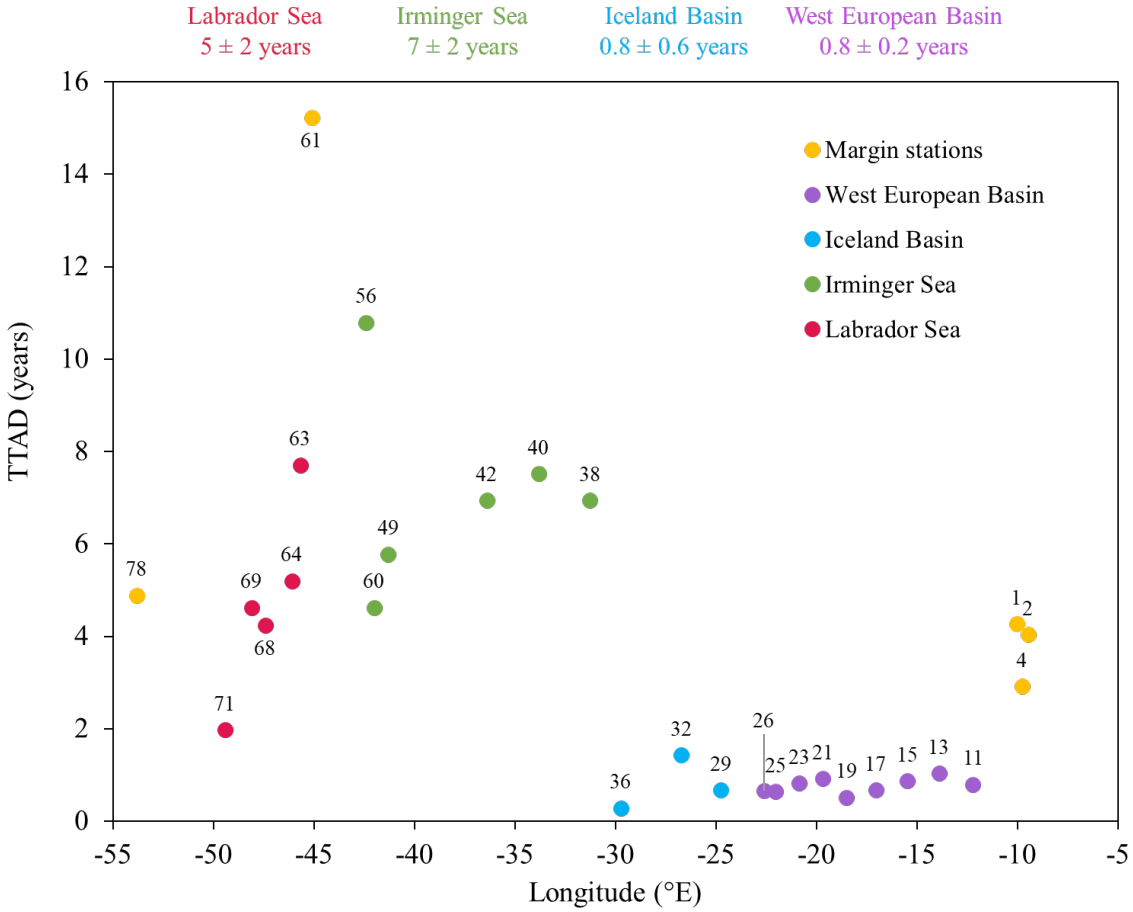

Figure 7: Section plot of the Fe* tracer in the North Atlantic Ocean with a remineralization rate ($R_{Fe:N}$) of 0.05 mmol mol^{-1} from surface to 225 m depth. A contour line of 0 separates areas of negative Fe* from areas with positive Fe*. Positive values of Fe* imply there is enough iron to support complete consumption of NO_3^- when this water is brought to surface, and negative Fe* values imply a deficit. See text for details.

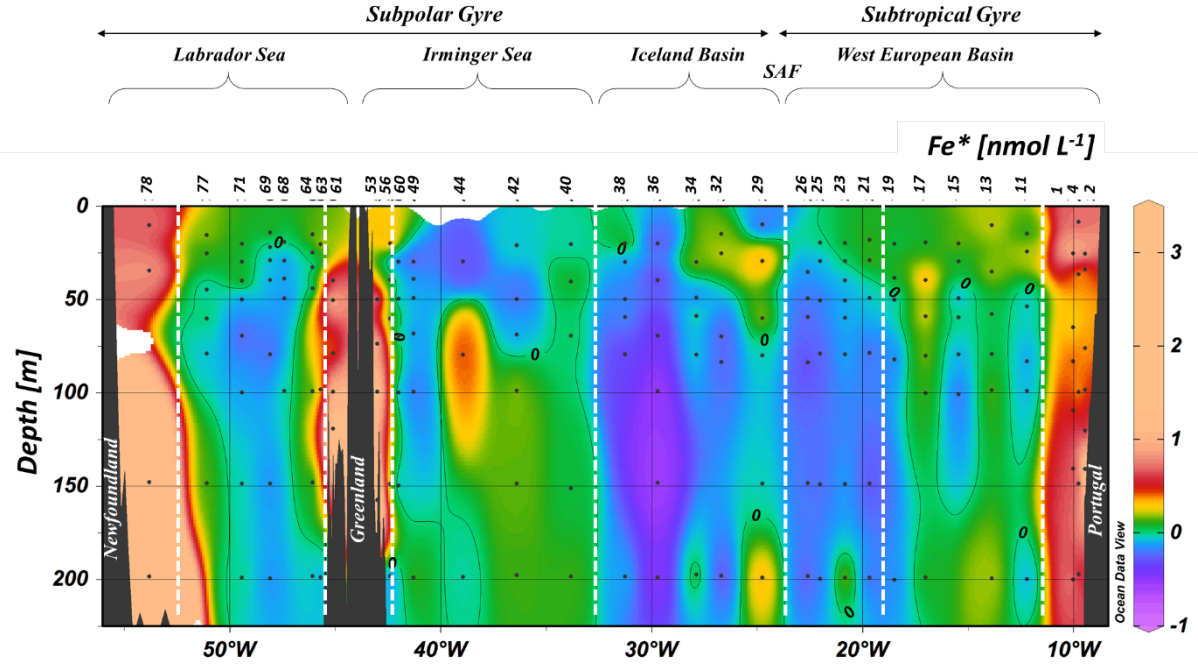

Table 1: Station number, date of sampling (in the DD/MM/YYYY format), size pore used for filtration (µm), station location, mixed layer depth (m) and associated average dissolved iron (DFe) concentrations, standard deviation and number of samples during the GEOTRACES GA01 transect. Note that the asterisk next to station numbers refers to disturbed temperature and salinity profiles as opposed to uniform profiles.

Station	Date sampling	filtration	Latitude	Longitude	Z_m	DFe (nmol L^{-1})			
	DD/MM/YYYY	µm	°N	°E	m	average		SD	n
1	19/05/2014	0.2	40.33	-10.04	25.8	1.07	±	0.12	1
2	21/05/2014	0.2	40.33	-9.46	22.5	1.01	±	0.04	1
4	21/05/2014	0.2	40.33	-9.77	24.2	0.73	±	0.03	1
11	23/05/2014	0.2	40.33	-12.22	31.3	0.20	±	0.11	2
13	24/05/2014	0.45	41.38	-13.89	18.8	0.23	±	0.02	1
15	28/05/2014	0.2	42.58	-15.46	34.2	0.22	±	0.03	2
17	29/05/2014	0.2	43.78	-17.03	36.2	0.17	±	0.01	1
19*	30/05/2014	0.45	45.05	-18.51	44.0	0.13	±	0.05	2
21	31/05/2014	0.2	46.54	-19.67	47.4	0.23	±	0.08	2
23*	02/06/2014	0.2	48.04	-20.85	69.5	0.21	±	0.05	6
25	03/06/2014	0.2	49.53	-22.02	34.3	0.17	±	0.04	2
26	04/06/2014	0.45	50.28	-22.60	43.8	0.17	±	0.03	2
29	06/06/2014	0.45	53.02	-24.75	23.8	0.17	±	0.02	1
32	07/06/2014	0.2	55.51	-26.71	34.8	0.59	±	0.08	2
34	09/06/2014	0.45	57.00	-27.88	25.6	NA	±		0

36	10/06/2014	0.45	58.21	-29.72	33.0	0.12	±	0.02	1
38	10/06/2014	0.45	58.84	-31.27	34.5	0.36	±	0.16	2
40	12/06/2014	0.45	59.10	-33.83	34.3	0.39	± P	0.05	1
42	12/06/2014	0.45	59.36	-36.40	29.6	0.36	±	0.05	1
44	13/06/2014	0.2	59.62	-38.95	25.8	NA	±		0
49	15/06/2014	0.45	59.77	-41.30	60.3	0.30	±	0.05	2
53*	17/06/2014	0.45	59.90	-43.00	36.4	NA	±		0
56*	17/06/2014	0.45	59.82	-42.40	30.0	0.87	±	0.06	1
60*	17/06/2014	0.45	59.80	-42.00	36.6	0.24	±	0.02	2
61*	19/06/2014	0.45	59.75	-45.11	39.8	0.79	±	0.12	1
63*	19/06/2014	0.45	59.43	-45.67	86.7	0.40	±	0.03	1
64	20/06/2014	0.45	59.07	-46.09	33.9	0.27	±	0.06	2
68*	21/06/2014	0.45	56.91	-47.42	26.3	0.22	±	0.01	1
69*	22/06/2014	0.45	55.84	-48.09	17.5	0.24	±	0.02	1
71	24/06/2014	0.45	53.69	-49.43	36.7	0.32	±	0.04	2
77*	26/06/2014	0.45	53.00	-51.10	26.1	NA	±		0
78	27/06/2014	0.45	51.99	-53.82	13.4	0.79	±	0.05	1

Table 2: SAFe S, GSP and NASS-7 dissolved iron concentrations (DFe, nmol L-1) determined by the SeaFAST-picoTM and their consensus (SAFe S, GSP; https://websites.pmc.ucsc.edu/~kbruland/GeotracesSaFe/kwbGeotracesSaFe.html) and certified (NASS-7; https://www.nrc-cnrc.gc.ca/eng/solutions/advisory/crm/certificates/nass_7.html) DFe concentrations. Note that yet no consensual value is reported for the GSP seawater.

Seawater used for calibration	Sea*FAST*-pico^{TM} DFe values (nmol L^{-1})				reference or certified DFe values (nmol L^{-1})		
	Average		SD	n	Average		SD
SAFe S	0.100	±	0.006	2	0.095	±	0.008
GSP	0.16	±	0.04	15	NA	±	NA
NASS-7	6.7	±	1.7	12	6.3	±	0.5

Table 3: Averaged DFe:DAl (Menzel Barraqueta et al., 2018) and PFe:PAl (Gourain et al., in prep.2019) ratios reported per margins. Note that to avoid phytoplankton uptake, only depth below 100 m depth are considered.

Margins	**Stations**	**DFe:DAl (mol:mol)**			**PFe:PAl (mol:mol)**			**DFe:PFe (mol:mol)**			**n**
	#	average		SD	average		SD	average		SD	
Iberian Margin	2 and 4	0.07	±	0.03	0.20	±	0.01	0.13	±	0.09	10
East Greenland Margin	56 and 53	0.21	±	0.09	0.30	±	0.01	0.12	±	0.03	6
West Greenland Margin	61	0.18	±	0.02	0.32	±	0.01	0.14	±	0.04	3
Newfoundland Margin	78	1.1	±	0.41	0.31	±	0.01	0.06	±	0.02	4